

# Induced nuclear activity in galaxy pairs with different morphologies (E+E), (E+S) and (S+S).

Francisco J. Hernández-Ibarra<sup>1\*</sup>, Yair Krongold<sup>1</sup>, Deborah Dultzin<sup>1</sup>,  
Ascensión del Olmo<sup>2</sup>, Jaime Perea<sup>2</sup>, Jesús González<sup>1</sup>,  
Sandro Mendoza-Castrejón<sup>1</sup> and Theodoros Bitsakis<sup>1</sup>

<sup>1</sup>*Instituto de Astronomía, Universidad Nacional Autónoma de México, Apartado Postal 70-264, 04510 México DF, México.*

<sup>2</sup>*Instituto de Astrofísica de Andalucía (C.S.I.C.) Apartado 3004, 18080 Granada, Spain.*

## ABSTRACT

We analysed 385 galactic spectra from the Sloan Digital Sky Survey Data Release 7 (SDSS-DR7) that belong to the catalog of isolated pairs of galaxies by Karachentsev. The spectra corresponds to physical pairs of galaxies as defined by  $V \leq 1200$  Km/s and a pair separation  $\leq 100$  kpc. We search for the incidence of nuclear activity, both thermal (star-forming) and non-thermal -Active Galactic Nuclei (AGN)-. After a careful extraction of the nuclear spectra, we use diagnostic diagrams and find that the incidence of AGN activity is 48 % in the paired galaxies with emission lines and 40% for the total sample (as compared to  $\sim 43$  % and 41% respectively in a sample of isolated galaxies). These results remain after dissecting the effects of morphological type and galactic stellar mass (with only a small, non significant, enhancement of the AGN fraction in pairs of objects). These results suggest that weak interactions are not necessary or sufficient to trigger low-luminosity AGN. Since the fraction of AGN is predominant in early type spiral galaxies, we conclude that the role of a bulge, and a large gas reservoir are both essential for the triggering of nuclear activity. The most striking result is that type 1 galaxies are almost absent from the AGN sample. This result is in conflict with the Unified Model, and suggests that high accretion rates are essential to form the Broad Line Region in active galaxies.

**Key words:** galaxies: active - galaxies: evolution - galaxies: interactions

## 1 INTRODUCTION

One of the outstanding problems in the understanding of the Active Galactic Nuclei (AGN) phenomenon is the feeding processes of the central Supermassive Black Hole (SMBH). The gas fueling may be driven from extragalactic to galactic, and further to nuclear scales. The main proposed mechanism to induce gas inflow to the centre of galaxies, on the extragalactic and galactic scales, consists primarily of interactions with other galaxies (Barnes & Hernquist 1992; Hopkins et al. 2005; Springel, Di Matteo, & Hernquist 2005; Cox et al. 2008; Ellison et al. 2008; Knapen & James 2009). In this paper we address observational evidence of the role of gravitational interactions in inducing nuclear activity.

### 1.1 Studying the Environment of AGN

In the past 20 years several efforts have focused in the study of the environment of AGN, in an attempt to elucidate this question from an observational point of view. Most of the investigations have dealt with samples of Seyfert galaxies, because these are the closest clearly non-thermal dominated active nuclei. Low Ionization Nuclear Emission Regions (LINERs) are easy to observe, however, the nature of the dominating emission mechanism is still debated (Krongold et al. 2003; González-Martín et al. 2007; González-Martín et al. 2015). Starburst phenomena (particularly circumnuclear) have also been included as a type (and/or part) of activity. The first authors to propose a Starburst-AGN connection were Perry & Dyson (1985). An excellent review on this topic can be found in Storchi-Bergmann (2008).

The first studies of the extragalactic influence on AGN, were devoted to investigate the difference in the environment between active and non-active galaxies, without distinguishing activity type, (Dahari 1984, 1985). But soon it became

\* E-mail:hibarra@astro.unam.mx

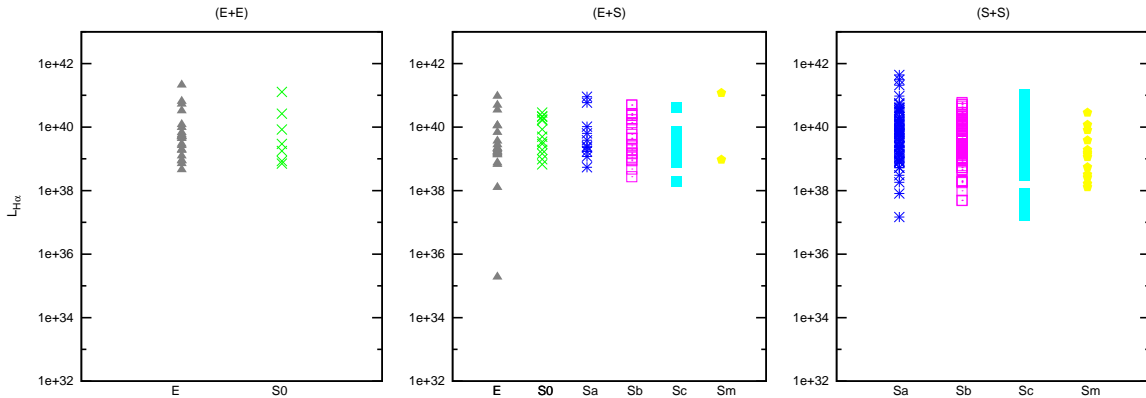


**Figure 1.** Morphological distribution of H $\alpha$  luminosity for: left; (E+E) sample, middle; (E+S) sample and right; (S+S) sample. Mean values of AGN H $\alpha$  luminosity for the three samples are  $L_{H\alpha} = 2.28 \times 10^{40} \text{ erg s}^{-1}$ ,  $L_{H\alpha} = 2.92 \times 10^{40} \text{ erg s}^{-1}$  and  $L_{H\alpha} = 1.44 \times 10^{40} \text{ erg s}^{-1}$  respectively.

clear that it was necessary to distinguish between type 1 and type 2 AGN (and even Starburst or enhanced Star Forming activity). More recently, the importance of making a difference between close and large scale environment has become clear. Seminal studies were affected by the lack of clear sample definitions, statistical biases and also biases introduced by sample selection effects. All these methodological problems yielded contradictory results that can be found in the literature for over more than 20 years; from Stauffer (1982b,a) to Koulouridis et al. (2013). One of the first discussions of these effects is given in Dultzin-Hacyan et al. (1999) hereafter DH99, and a detailed account of these different results is reviewed and analyzed by Sorrentino et al. (2006).

As more refined studies have been performed, it has become clear that Seyfert 2 galaxies are in interaction with the same frequency than Star-Forming Galaxies (SFG) (Krongold et al. 2001; Storchi-Bergmann 2008), while Seyfert 1 galaxies are in interaction less frequently. Seyfert 1s are found with close companions comparably as often as non-active galaxies (Krongold et al. 2002, DH99). The most recent studies confirm these findings considering only physical companions, i.e. not only from statistical considerations, but from actual measurements of radial velocities for the neighboring galaxies (Koulouridis et al. 2006a,b). From a statistical point of view, Sorrentino et al. (2006) have made the comparison of the environment of AGN, SFG and normal galaxies, for a complete sample of 1829 Seyfert galaxies (725 Sy1 and 1104 Sy2) and 6061 SFG from the Fourth Data Release (DR4) of the SDSS. This study fully confirms the results found by DH99 and by Koulouridis et al. (2006a,b). The authors state that for close systems ( $\leq 100$  kpc) they find a higher fraction of Sy2 compared to Sy1 in agreement with DH99, moreover, the frequency of Sy2 is similar to that of SFGs. The most recent confirmation of this result comes from Villarroel & Korn (2014). At large scales however, there is no strong evidence of a denser environment for AGN compared to “normal” galaxies, in agreement with Schmitt (2001) and Koulouridis et al. (2006a). Any difference in the large-scale environment of Sy2 and Sy1 is more related to the morphological type of the host rather than to activity (see also Márquez & Masegosa 2008).

## 1.2 A Complementary Approach: Studying the Incidence of Nuclear Activity in Interacting Galaxies

In all of the former analysis, the environment of well defined samples of active vs. non-active galaxies were compared. In the present paper we adopt a complementary approach. We study the incidence of nuclear activity in a well defined sample of interacting galaxies. We focus on the sample of the Catalogue of Isolated Pairs in the Northern Hemisphere (Karachentsev 1972). In order to quantify the incidence of nuclear activity in the pairs of our sample, we distinguish three morphological pairs; 1) Elliptical plus Elliptical pair (E+E) considering spherical morphology S0, 2) Elliptical plus Spiral pair (E+S) and 3) Spiral plus Spiral pair (S+S)

There has been efforts in the literature to assess the incidence of AGN in pairs of galaxies. Galaxies in elliptical pairs (E+E) have shown an enhancement on the level of recent star formation relative to a control sample of early-type galaxies (Rogers et al. 2009). After a first stage of an encounter that triggers residual star formation, a more efficient inflow of gas towards the centre may switch the object to an AGN phase. Thus the possibility that external perturbations may enhance the frequency of nuclear activity among galaxies has been suggested by previous studies (Dultzin-Hacyan et al. 1999; Krongold et al. 2002, 2003; Rogers et al. 2009; Ellison et al. 2011; Villforth, Sarajedini, & Koekemoer 2012; Liu et al. 2012) and supported later by mid-IR spectroscopy (e.g. Mendoza-Castrejón et al. 2015).

Mixed galaxy pairs (E+S) are a unique laboratory to study the effect of tidal forces in triggering nuclear activity because they are relatively simple systems where a gas rich galaxy interacts with a gas poor one. In such systems a clean interpretation of the origin and evolution of the fueling material is possible. Mixed pairs minimize the role of the relative orientation and pair component spin vectors, in driving interaction-induced effects (Keel 1993). Since the late-type spiral component is the primary source of gas in a mixed pair, it is therefore expected to be the site of all or most star formation and nuclear activity, although recent results have shown evidence of star formation and AGN activity

in a non-negligible fraction of the early type components of the pairs (de Mello et al. 1995, 1996; Domingue et al. 2005, based on IRAS data). The presence of AGN activity on the early type components can be directly confirmed by means of spectroscopic data (Dultzin et al. 2008; Coziol et al. 2011; Sabater et al. 2012).

Previous studies, based on spiral-spiral pairs (S+S), have shown that starburst and possibly AGN activity in galaxies may be triggered by interactions. Kennicutt & Keel (1984) studied a sample of 56 nearby spirals in pairs vs. a control sample of 86 non-interacting galaxies, and found that interactions induce an enhancement of the level of nuclear activity. Furthermore, they also found a significant fraction of Seyfert or Seyfert-like type nuclei. However, these studies have searched for activity without distinguishing between thermal (starburst, hereafter SB) and non-thermal (properly an AGN) activity. Thus they have not addressed the incidence of type 1 vs. type 2 AGN in pairs of galaxies.

The incidence of AGN in groups have also been addressed by several authors.

Martínez et al. (2008, 2010) studied compact groups of galaxies, consisting of associations of 4 galaxies or more with very high local densities in an rather isolated large scale environment. A high frequency of nuclear activity is observed for 270 galaxies in 64 Hickson compact groups. In particular it is found that among the emission line galaxies (63% of the whole sample), 45% show a pure AGN, 23% have a composite spectrum and 32% show nuclear star formation. In all cases, the nuclear activity is manifested as low luminosity AGN and there is a statistically significant deficiency of type 1 AGN as compared to field galaxies. Bitsakis et al. (2015) study the evolution of the nuclear activity and how it has been affected by the dense environment of the groups. Their analysis is based on the largest multiwavelength compact group sample to-date. They observe that over the past 3 Gyr, there has been an enhancement of 15% in the number of the AGN-hosting late-type galaxies. This enhancement is accompanied by the corresponding decrease of their circum-nuclear star formation. These authors also show that at any given stellar mass, galaxies found in dynamically old groups are more likely to host an AGN, than those in young groups.

When going to richer environments, such as clusters of galaxies, the AGN fraction decreases. However, the results seem to depend on the methods to search for the AGNs. In X-rays, AGNs are detected with low fraction (~5-8%; Martini, Mulchaey, & Kelson 2007), with an increasing frequency at higher redshift and AGN luminosity (Martini et al. 2013). In the optical Popesso & Biviano (2006) found a LLAGN fraction of 15 to 21%, when analysing SDSS spectroscopy of 324 nearby clusters. They report a clear increasing trend of the AGN fraction as the cluster velocity dispersion decreases and the merging rate increases. All these richness of results clearly indicates that in order to elucidate the exact effect of interactions on triggering AGN, it is mandatory to go to systems such as isolated pairs of galaxies, where the effects of single galaxy-galaxy encounters (and the lack of further perturbations) can provide a clear answer.

In this work, we study the incidence of nuclear activity in a well defined sample of galaxy pairs. Host spectra galaxy extraction and line emission measurements have been performed systematically in order to make a good quantification

of the data. We define the activity type of AGN and separate between Seyfert and LINER nuclei.

In the following section we present the sample and data analysis (§2), where an optical classification by diagnostic diagrams is performed. On §3 we present our results on the incidence of nuclear activity. Discussion takes place on §4. On section 5 we present the final conclusions of this work. Throughout the paper, we compare our results on pairs of galaxies, with those of a rigorously defined sample of isolated galaxies (results by our group: Hernández-Ibarra et al. 2013, hereafter H-I13). The methods and analysis between H-I13 and this work are fully self-consistent, which warrants a direct and reliable comparison. H-I13 analyze to different samples of isolated galaxies. Throughout the paper we compare with the results over the sample defined with the catalogue of isolated galaxies (CIG; Karachentseva 1972), for which we obtain more reliable results (as discussed in H-I13).

## 2 SAMPLE AND DATA ANALYSIS

This study is based on the Catalog of Isolated Pairs of galaxies (Karachentsev 1972, CPG) that contains nearly 600 galaxy pairs. The catalogue is based on a visual search of the Palomar Sky Survey with  $\delta \geq -3^\circ$ . The majority of the objects have high galactic latitude  $b \geq 20^\circ$  (in order to avoid galactic extinction) and magnitude limit  $m_{Zw} \leq 15.7$ . Karachentsev (1972) used a strong pair-isolation criterion in terms of the apparent angular separation between pairs ( $\leq 100$  Kpc). The criteria used to build the CPG can be resumed by the following relations:

$$\frac{x_{ij}}{x_{12}} \geq \frac{5a_i}{a_j}; \quad 0.5a_j \leq a_i \leq 4a_j \quad (1)$$

where  $j = 1, 2$  correspond to the pair components and  $i$  is the nearest neighbour,  $a$  represents the major-axis diameter and  $x$  the apparent separation. The overall completeness of this catalogue has been estimated in  $\sim 90\%$  (Hernández Toledo et al. 1999).

We obtain all the available spectra for our sample from the Sloan Digital Sky Survey Data Release 7 (SDSS-DR7) (Abazajian et al. 2009). The spectra have a wavelength coverage from 3800-9200Å and a resolution of 1800-2200 with a signal-noise  $>4$  per pixel at  $g=20.2$ . We find that 99% of the objects in our sample have a r-magnitude brighter than the SDSS spectroscopic limit ( $r = 17.77$ ), thus our sample has a high completeness. We note that in several cases, only one of the member of the pairs have spectroscopic data, and thus, only that object is included in the analysis. The total sample consists of 385 galaxies for which spectral data is available. Tables A1, A2, and A3 present the samples for the different types of pairs.

We note that the SDSS spectra were taken through a fibre aperture of 3 arcsec in diameter (corresponding to 1.25 kpc at a redshift of 0.02). This guarantees that the nuclear region of the galaxies was observed. However, the collected integrated spectroscopic area is large enough to include stellar light contamination. This contamination turns out to be more significant at the central parts of the galaxies as the spheroidal/bulge component becomes more relevant. There-

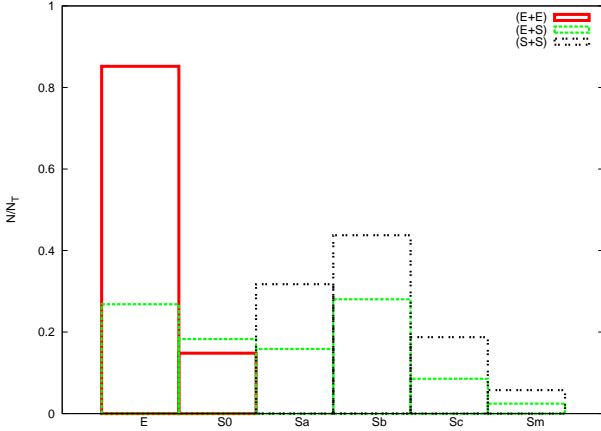


**Figure 2.** Morphological distribution of galaxies in elliptical, mixed and spiral pairs. Continuous red line correspond to (E+E) pair sample, green dashed line to (E+S) and black dotted line to (S+S) pair samples.

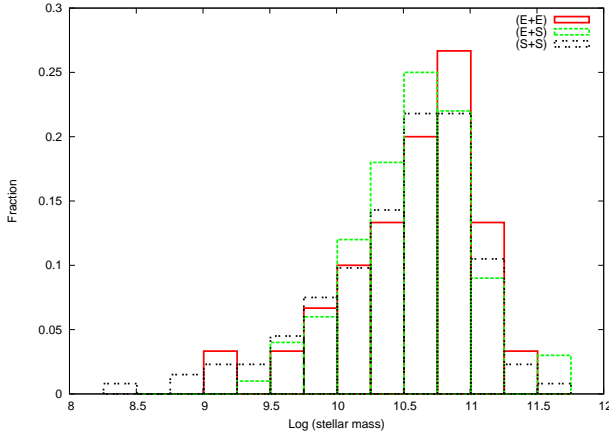


**Figure 3.** Mass distribution for the three subsample galaxy pairs. Labels like in Fig. 2.

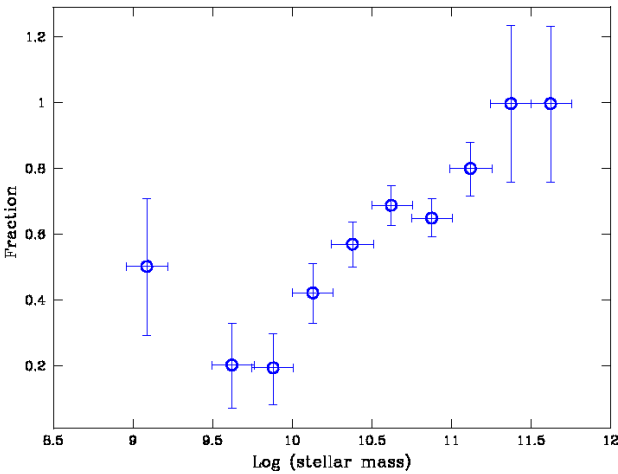


**Figure 4.** AGN fraction of galaxies as a function of stellar mass. AGN are show as blue empty circles. Errors in y-direction are the standard deviation per bin and the “error bars” in x-direction denote the range of mass in each bin.

fore, in order to obtain a reliable nuclear classification based on the emission lines it is mandatory to subtract the stellar contribution. We applied the principal component analysis (PCA) method following Hao et al. (2005) to subtract this contribution. We used their first 8 eigenspectra from their low redshift range. These eigenspectra are the resulting eigenvectors of a PCA analysis applied to a sample of high S/N spectra of non-emission galaxies. In addition, as they pointed out, we included two more components, an A star spectrum accounting for the possible presence of post-starburst features and a power-law to take into account the possible existence of a non-thermal component. The analysis is performed for all the spectra of our sample and it consists on a multiple regression of each spectrum to a linear combination of the 8 eigenspectra plus the two additional components. Previously to the fit each galaxy spectrum was moved to zero redshift which is the one of the template library. We also masked all those regions where emission lines may appear since the quality of the fit lies on the matching of the continua. Once the regression is performed, the direct subtraction of the resulting fit to the original ( $z=0$ ) spectrum provides us with a pure emission line spectrum where all the underlying absorption components and eventually a non thermal component of the continuum are removed.

With a clean emission line spectrum at hand, we focused in measuring the intensity of the 7 strongest emission lines:  $H\beta$ ,  $[O\ III]\ \lambda 5007$ ,  $[O\ I]\ \lambda 6300$ ,  $H\alpha$ ,  $[N\ II]\ \lambda 6584$  and  $[S\ II]\ \lambda\lambda 6717,31$ . We consider clear line detections those features with a signal to noise ratio ( $S/N$ )  $\geq 3$ . In our measurements, we were careful to distinguish between intrinsic no detected emission (to a given flux limit) and a lack of detectability related to low S/N data. For this purpose, we set a threshold of  $10^{38}\ \text{erg s}^{-1}$  in the  $H\alpha$  luminosity. We consider galaxies below this threshold as true non-emission objects (according to our results, the probability that a galaxy with such low  $H\alpha$  luminosity is an AGN is less than 2%, which gives high robustness to our results). Objects with no detected lines, but a  $3\sigma$  upper limit larger than this threshold in the  $H\alpha$  line are not included in the results, as it is not clear whether these are no-emission line galaxies, or just objects with poor data quality. In this way a systematic and self-consistent luminosity limited analysis is warranted. The distribution of morphology and  $H\alpha$  luminosity of our sample (presented for each morphological pair type) are presented in Fig. 1.

From our 385 spectra, 63 are true non-emission objects, 9 do not have all the 7 emission lines detected with a significance above  $3\sigma$ , 4 have problems with the host galaxy spectra subtraction, and 1 does not have the optic fibre in the galaxy centre. Objects with detections below  $3\sigma$ , without good subtraction and with the fibre off the center were not included in this work (14 objects).

Fluxes were calculated with the Sherpa software (<http://cxc.cfa.harvard.edu/sherpa/>) which comes in the CIAO distribution, <http://cxc.harvard.edu/ciao/>. This program fits emission lines with Gaussians.

We evaluated the line intensities using two methods to fit the lines (see full description in H-I13). The first one consisted in constraining the width and velocity to the same value in our fits for two separated groups of lines, forbidden and permitted. Therefore, these fits included four free parameters in our models: the width and velocity of the forbidden and the permitted lines. An additional free pa-

parameter for each line in the model was the intensity. The second method constrains the width and velocity for all the detected lines (independently of whether they were permitted or forbidden) to have the same value (i.e. only two free parameters to model all lines) plus an additional free parameter for the intensity of each line. Our results show that both methods are equivalent without any substantial difference. We report here the emission line intensities obtained with the second method that has less free parameters. We note that for those objects where a broad component was required in addition to the narrow one, an individual broad Gaussian was fitted with fully independent free parameters.

Figs. 2 and 3 show the morphological type and mass distributions respectively for the galaxies in the three subsamples of galaxy pairs. In Fig. 4 we show the AGN and HII activity fraction versus the logarithm of stellar mass per bin, derived for our entire sample.

## 2.1 Optical classification

The optical classification was performed using diagnostic diagrams (Baldwin et al. 1981; Veilleux & Osterbrock 1987). Using the 7 emission lines measured, diagnostic diagrams were constructed with the aid of line ratios  $[\text{O III}]/\text{H}\beta$ ,  $[\text{N II}]/\text{H}\alpha$ ,  $[\text{S II}]/\text{H}\alpha$  and  $[\text{O I}]/\text{H}\alpha$ .

We based our activity type classification on the  $([\text{N II}]/\text{H}\alpha)$  versus  $([\text{O III}]/\text{H}\beta)$  diagnostic diagram (hereafter  $[\text{N II}]$  diagram), which is the main diagnostic to distinguish objects with different nature. However, we have used the  $([\text{S II}]/\text{H}\alpha)$  versus  $([\text{O III}]/\text{H}\beta)$  diagnostic diagram (hereafter  $[\text{S II}]$  diagram) to separate between star-forming galaxies, Seyfert galaxies and LINERs. We have chose to do this, rather than using the Schawinski et al. (2007) diagnostic over the  $[\text{N II}]$  diagram in order to keep the results of this work consistent with those by H-I13. We note, nevertheless, that the  $[\text{N II}]$  and  $[\text{S II}]$  diagrams give consistent results. We do not use the  $([\text{O I}]/\text{H}\alpha)$  versus  $([\text{O III}]/\text{H}\beta)$  diagnostic diagram (hereafter  $[\text{O I}]$  diagram) to classify our objects, considering the relative weakness of this line. However, we keep the results based  $[\text{O I}]$  diagram throughout the paper for completeness. We further notice that we consider AGN all objects meeting the requirements described above, and a large fraction of these may be LINERs. Thus, some of these objects might be powered by other processes rather than accretion (§1).

In Figure 5, we present diagnostic diagrams for the ( $E+E$ ) pair sample. Panel (a) shows the  $[\text{N II}]$  diagram. We define different regions to separate galaxies with an AGN, composite galaxies (whose ionization fractions contain contributions from both an AGN and star formation processes), and star forming galaxies (we do not distinguish starburst from star forming galaxies, as this would require a robust measurement of the star formation rate). We use the “maximum starburst line” (Kewley et al. 2001, hereafter Ke01), to separate galaxies with an AGN from star forming objects (green dashed line in Fig. 5a), and the empirical line from Kauffmann et al. (2003, hereafter Ka03) to distinguish between pure star forming galaxies from AGN-star-forming composite objects (continuous red line). Galaxies between the two classification lines are the composite objects, meaning that they contain metal-rich stellar population and AGN

features in their spectra. They consist of a circumnuclear star forming region surrounding a Seyfert or LINER nucleus.

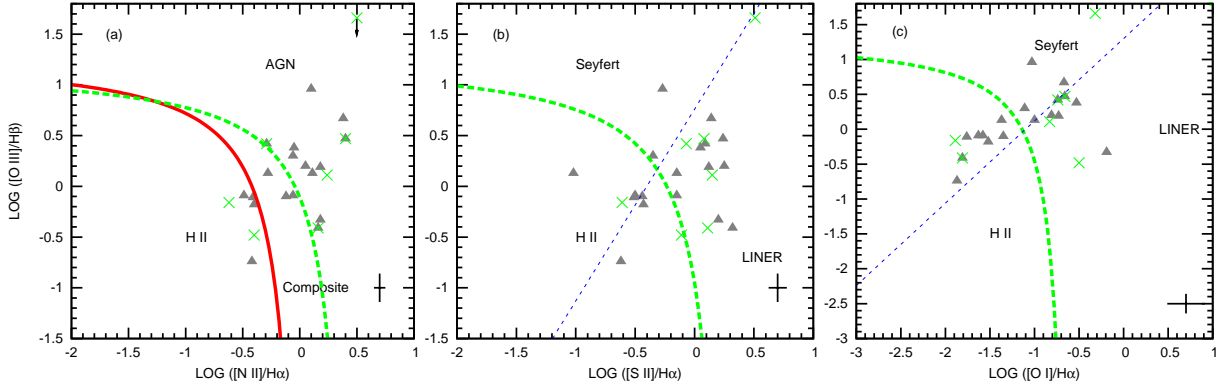
Panel (b) presents the  $[\text{S II}]$  diagram, that as explained above, was used to separate between star-forming galaxies, Seyfert galaxies and LINERs. The green line corresponds to Ke01. The dashed blue line (Kewley et al. 2006, hereafter Ke06) separates AGN activity between Seyfert and LINER. On this diagram, objects above Ke01 line can be Seyfert objects (above Ke06 line) or LINERs (objects below Ke06 line). Panel (c) shows the  $[\text{O I}]$  diagram.

Fig. 6, shows the  $[\text{N II}]$ ,  $[\text{S II}]$  and  $[\text{O I}]$  diagrams for the ( $E+S$ ) pair sample. Similarly Figs. 7, 8, and 9 show the  $[\text{N II}]$ ,  $[\text{S II}]$  and  $[\text{O I}]$  diagnostic diagrams for the ( $S+S$ ) pair sample. In all these plots, we use different symbols to identify galaxies with different morphological classification to study the distribution of AGN among every Hubble type.

In this work, we consider composite galaxies as AGN, because they require a non-thermal continuum component to produce the level of ionization detected in their lines, that indicates the presence of (low) accretion rates into black holes. This is further supported by the fact that composite galaxies present a X-ray hard emission, and are considered AGN in other types of diagnostic diagrams such as the TBT diagram (see Trouille et al. 2011).

## 2.2 Morphological Classification

As mentioned earlier, we check the morphological classification of the galaxies in our sample. In a few cases the morphology was changed from that in the literature. These are outlined below. We find that KPG 466B is clearly a spiral in the Sloan image and thus is considered in the ( $S+S$ ) sample. According to NED, KPG 167A has elliptical type, but a spiral structure is evident from the Sloan image. KPG 167B belongs to the Sb type according NED, yet it can be clearly seen as an elliptical in the SDSS. KPG 466A presents emission lines with a double component, in both the permitted and forbidden lines. This might be due to a circumgalactic ring that can be clearly distinguished in the Sloan image. Finally, the morphological classification of KPG 419A was obtained from a surface photometry study by Franco-Balderas et al. (2004) in order to avoid the existent ambiguity between NED, SIMBAD and HYPERLEDA data. We further checked the morphology of our galaxies with those classifications in the Galaxy Zoo (Lintott et al. 2008) and in the Nair & Abraham (2010) samples. As described in Lintott et al. (2008), we only used the morphological classifications of Galaxy Zoo with  $>80\%$  confidence. However, only a fraction of our galaxies were available in those catalogs (250 in Galaxy Zoo and 120 in Nair & Abraham, with 118 being common). Comparing these classifications with the ones we use in the paper, we find an agreement for  $>75\pm 4\%$  of the ellipticals and S0s, and  $\sim 95\pm 4\%$  of the Spirals. Interestingly, when comparing the classifications of Galaxy Zoo and Nair & Abraham for our 118 galaxies they have in common, we find they disagree in about 10% of them (with a larger disagreement in early types), thus stressing the difficulty of classifying the morphologies of galaxies using various methods.



**Figure 5.** Diagnostic diagrams of galaxies in (E+E) pairs. (a) The [N II] diagnostic diagram. (b) The [S II] diagnostic diagram. (c) The [O I] diagnostic diagram. Blue dashed line represents Seyfert/LINER line. Elliptical galaxies can be seen on filled gray triangles, lenticular on green crosses and the black crosses down on the right represents the mean error data.

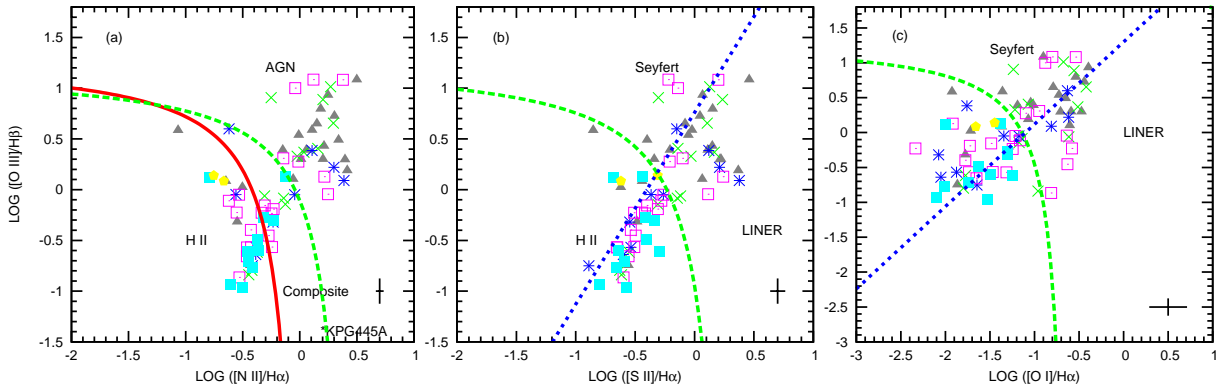


**Figure 6.** The [N II] diagnostic diagram for (E+S) pair sample. Morphological classification is show to every object, elliptical galaxies can be seen on filled gray triangles, lenticular on green crosses, Sa on blue asterisks, Sb red squares with point, Sc filled cyan squares and Sm yellow pentagons. Mean error data are represented by the black cross down at right.

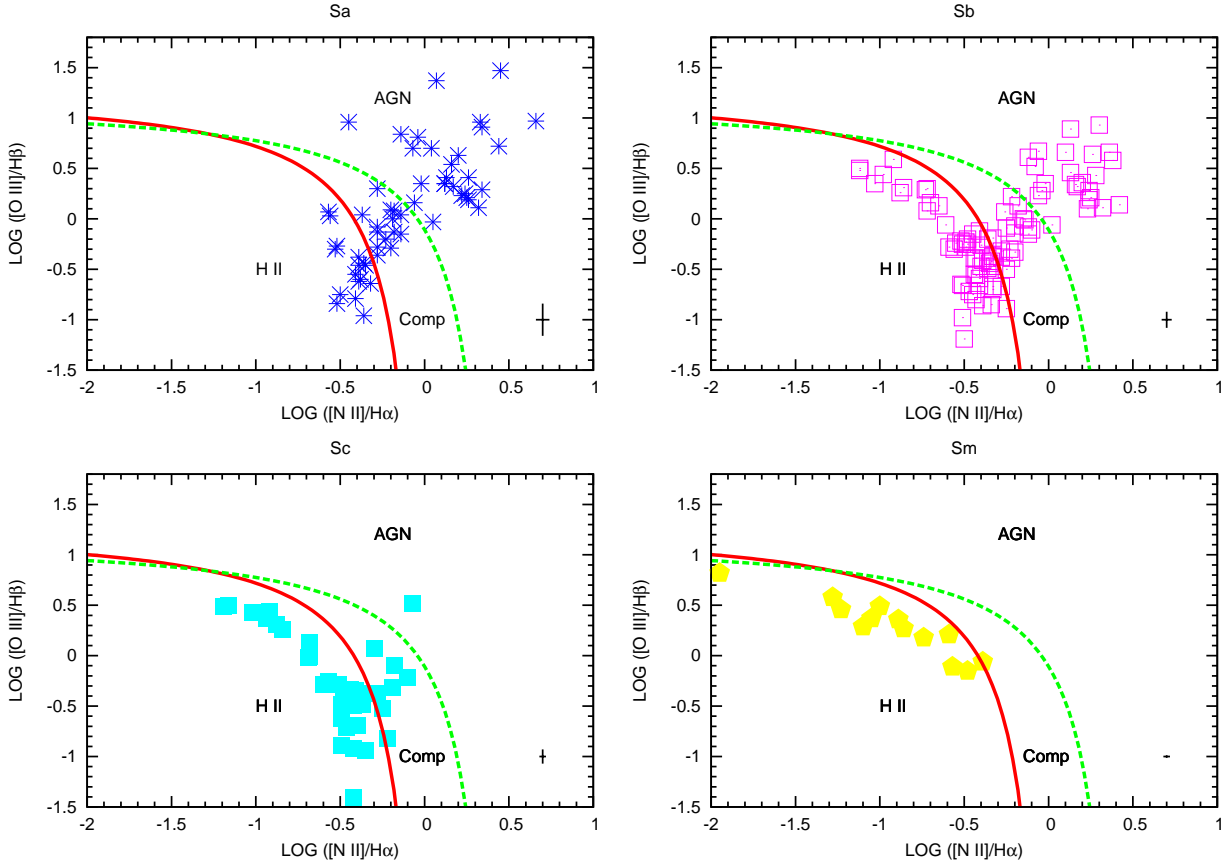
### 2.3 Stellar Mass of the Galaxies in the Samples

The stellar masses were calculated using the formula described in Bell et al. (2003, ApJS 149, 289). In this case we have used 2MASS K-band fluxes (thus,  $a_K = -0.283$ ,  $b_K = 0.091$ ), since they probe the old stellar populations which contribute the most to the stellar mass of galaxies. For the color parameter, we have used the u'-r' colors of the SDSS. The distribution of the redshift in our galaxies is  $0.00052 < z < 0.0491$  (thus they are local). Since we are using 2MASS K-band to constrain the stellar mass of the galaxies, there is no need to scale to total fluxes from SDSS. We also note that at this band the extinction from dust is minimum. We cross-correlate our stellar masses with those presented in SDSS DR10 (the 97.5 percentile total stellar masses) which were estimated using the method described in Kauffmann et al. (2003). Since Bell et al. (2003) is using a Salpeter IMF and Kauffmann et al. (2003) is using Krupa IMF, we multiply the second by a factor of 1.5 to convert them into Salpeter. Stellar masses calculated with both methods are very similar and they display a dispersion of 0.15dex (Bell et al. reports an expected scatter of 0.1-0.2dex). However,

towards stellar masses lower than  $10^{10} M_{\odot}$ , there is a systematic overestimation of the Bell et al. (2003) method by 0.35dex. This difference could originate from the different calibrations in the estimators, but has a negligible effect in our results.

## 3 RESULTS

Tables 1 to 3, show our results using the [N II] diagnostic diagram for the (E+E), (E+S), and (S+S) pairs of galaxies, respectively. These Tables present the fraction of AGN, composite, and star formation objects as a function of morphological type. The type of nuclear activity (LINER or Seyfert), obtained with the [S II] and [O I] diagnostic diagrams for the different samples of paired galaxies, are shown in Tables 4, 5, and 6. Finally, Table 7 summarizes our main findings in an easy and comparative way, showing the fraction of AGN as a function of morphological type of each object for our three samples of pairs. In this Table we also present the results from the sample of isolated galaxies by H-II13, for comparison.


**Figure 7.** Diagnostic diagram  $[\text{N II}]$  for galaxies in ( $S+S$ ) pairs.

**Table 1.** Morphology distribution and incidence of nuclear activity in ( $E+E$ ) pair sub-sample derived from  $[\text{N II}]$  BPT diagnostic diagram.

M.T.	Galaxies with Emission lines				Total sample			
	Total	Star-forming	Comp	AGN+Comp	Total	Star-forming	Comp	AGN+Comp
E	18	5(28%)	3(17%)	13(72%)	41	5(12%)	3(7%)	13(32%)
S0	7	2(29%)	1(14%)	5(71%)	14	2(14%)	1(7%)	5(36%)
Total	25	7(28%)	4(16%)	18(72%)	55	7(13%)	4(7%)	18(33%)

**Table 2.** Morphology distribution and incidence of nuclear activity in ( $E+S$ ) pair sub-sample derived from  $[\text{N II}]$  BPT diagnostic diagram.

M.T.	Galaxies with Emission lines				Total sample			
	Total	Star-forming	Comp	AGN+Comp	Total	Star-forming	Comp	AGN+Comp
E	21	5(24%)	0(0%)	16(76%)	33	5(15%)	0(0%)	16(48%)
S0	13	3(23%)	3(23%)	10(77%)	19	3(16%)	3(16%)	10(53%)
Sa	10	4(40%)	3(30%)	6(60%)	13	4(31%)	3(23%)	6(46%)
Sb	21	8(38%)	6(29%)	13(62%)	21	8(38%)	6(29%)	13(62%)
Sc	11	8(73%)	3(27%)	3(27%)	11	8(73%)	3(27%)	3(27%)
Sm	2	2(100%)	0(0%)	0(0%)	2	2(100%)	0(0%)	0(0%)
Total	78	30(38%)	15(19%)	48(62%)	99	30(30%)	15(15%)	48(48%)

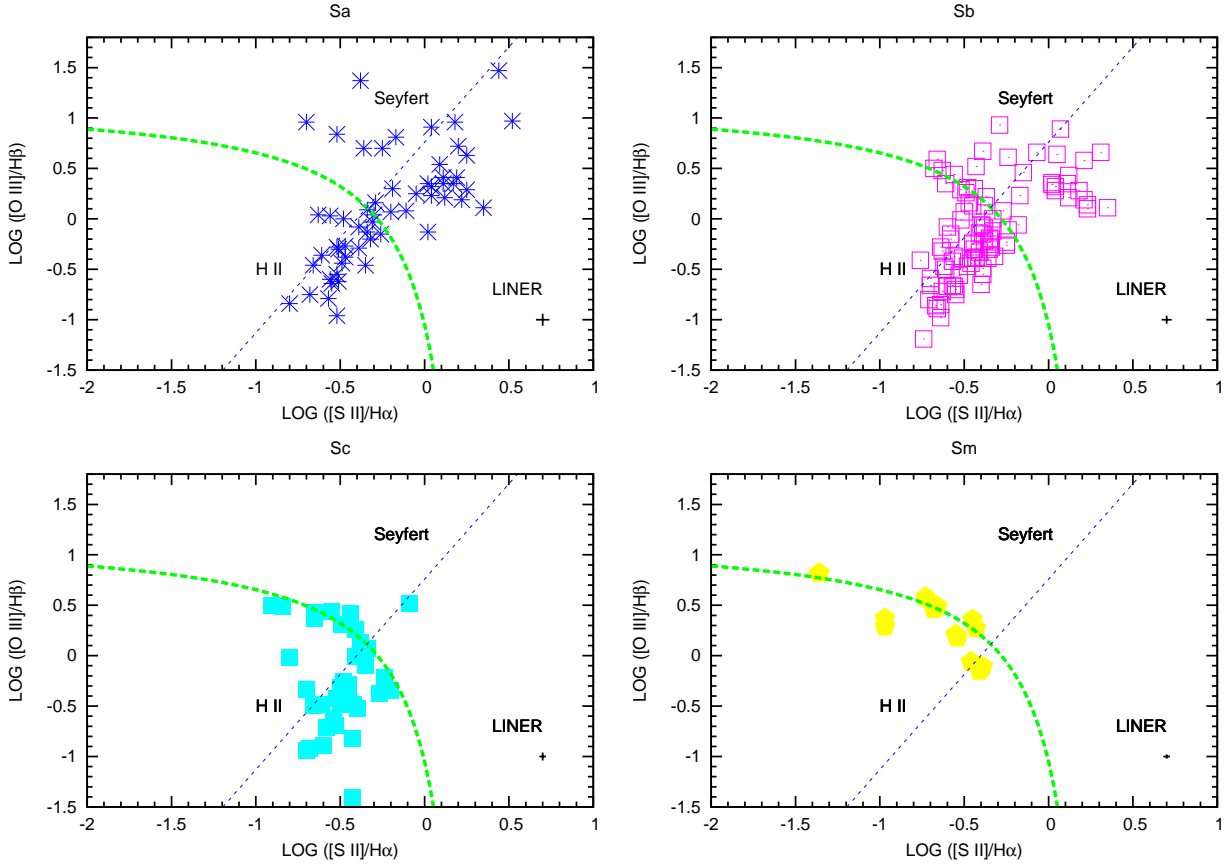


**Figure 8.** Diagnostic diagram [S II] for galaxies in (S+S) pairs.

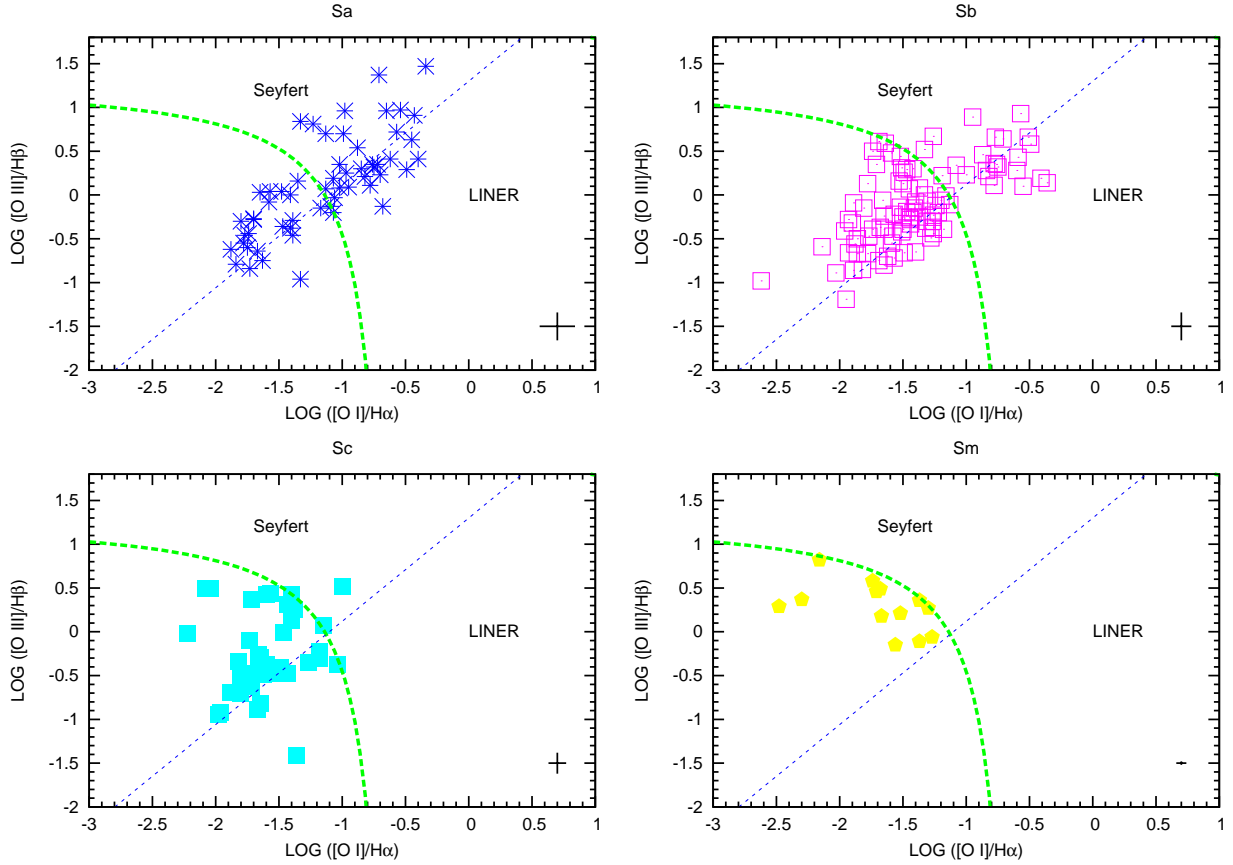
**Table 3.** Morphology distribution and incidence of nuclear activity in (S+S) pair sub-sample derived from [N II] BPT diagnostic diagram.

M.T.	Galaxies with Emission lines				Total sample			
	Total	Star-forming	Comp	AGN+Comp	Total	Star-forming	Comp	AGN+Comp
Sa	60	22(37%)	12(20%)	36(60%)	65	22(34%)	12(18%)	36(55%)
Sb	92	54(59%)	16(17%)	38(41%)	97	54(56%)	16(16%)	38(39%)
Sc	39	33(85%)	6(15%)	6(15%)	40	33(83%)	6(15%)	6(15%)
Sm	12	11(92%)	1(8%)	1(8%)	12	11(92%)	1(8%)	1(8%)
Total	203	120(59%)	35(17%)	83(40%)	214	120(56%)	35(16%)	83(39%)

Our results indicate that 48% of the emission line galaxies in pairs show the presence of nuclear (non-thermal) activity. When galaxies that do not show emission lines (according to the quantitative definition given in §2) are included in the calculations, this frequency decreases to 40%. We can compare this incidence with the sample of isolated galaxies by H-I13. Isolated objects with emission lines present nuclear activity in  $\sim 43\%$  of the cases, and  $\sim 41\%$  for the total sample (again, including non-emission galaxies; we note here that the definition of non-emission galaxies follows a self-consistent approach in this paper and in H-I13). This difference is clearly not statistically significant, indicating that interactions are not a sufficient condition in producing nuclear activity. However, it is important to note that these results are based on our complete sample, and kind of interaction in the pairs (S+S, E+E, or E+S), as well as morphological and mass distributions among the different samples

are different. Thus, the results on the total sample might be led by these different properties. One of the aims of the present work is precisely to separate these different effects.

Table 7 presents our results as a function of type of interaction for the different morphological classification of the objects. It can be observed that late type galaxies in (S+S) pairs have similar frequency of AGN than isolated galaxies. However, spirals in (E+S) pairs type galaxies have a frequency  $\sim 10\%$  larger than (S+S) and isolated galaxies. These results do not change if only galaxies with emission lines or the total samples are considered. The difference between the (E+S) pairs and the isolated and (S+S) pairs is of the order of the Poisson error in the measurements (10%), so not significant. As can be observed in the Table, the difference is mainly driven by the larger fraction of AGN in Sb galaxies that are members of the (E+S) pairs, that host an AGN 15-20% more often than Sb galaxies in the other


**Figure 9.** Diagnostic diagram [O I] for galaxies in ( $S+S$ ) pairs.

**Table 4.** Incidence type of nuclear activity for different morphologies from [S II] and [O I] diagnostic diagrams for ( $E+E$ ) sample.

M.T.	[S II] Diagram				[O I] Diagram			
	Total	AGN	Seyfert	LINER	Total	AGN	Seyfert	LINER
E	18	12(67%)	2(11%)	10(56%)	18	10(56%)	5(50%)	5(50%)
S0	7	5(71%)	0(0%)	5(100%)	7	5(71%)	1(20%)	4(80%)
Total	25	17(68%)	2(12%)	15(88%)	25	15(60%)	6(40%)	9(60%)

groups. However, due to the smaller number statistics, the Poisson error on this sample is similar to the difference. Observing at early type galaxies with emission lines in ( $E+S$ ) and ( $E+E$ ) pairs, we can observe that they have a high fraction of AGN in their nuclei, but comparable with the frequency observed in isolated galaxies. When galaxies without emission features are considered, the fraction decreases, but remains similar among the samples, with the only difference that galaxies in ( $E+E$ ) pairs seem to have a  $\sim 2\sigma$  (17-18%) smaller fraction of active galaxies.

Overall, it is clear from Table 7 that the main factor in the presence of AGN in galaxies is the morphological type. If only emission line objects are considered, Early type galaxies have the largest fraction, decreasing monotonically as the galaxies are of later type. However, when all objects are taken into account, the fraction of AGN in early types decreases, and the largest fraction of AGN are found in Sa and Sb galaxies.

As shown by H-I13 the mass of the galaxies is another dominant factor in determining the AGN fraction in galaxies. We find the same trend in our samples of paired galaxies. As can be seen in Figure 4, for galaxies with masses larger than  $10^{10.5}M_{\odot}$ , the fraction of galaxies hosting an active nucleus raises above 50%. For masses larger than  $10^{11}M_{\odot}$ , nearly all objects have an AGN component. Given that there is some relation between the morphological and the mass distributions in galaxy samples this result is not entirely surprising. However, there is more to it than this simple link between morphology and mass. A direct comparison (independent on morphology) suggests that paired galaxies in massive objects tend to host AGN more often than isolated galaxies at a single mass value, as observed in Figure 10. However, when one takes into account both the morphology and mass distribution in the samples this strong difference vanishes. This is observed in Figure 11, where the fraction of AGN is plotted for early and late type galaxies (as function

**Table 5.** Incidence type of nuclear activity for different morphologies from [S II] and [O I] diagnostic diagrams for (E+S) sample.

M.T.	[S II] Diagram				[O I] Diagram			
	Total	AGN	Seyfert	LINER	Total	AGN	Seyfert	LINER
E	21	16(76%)	5(31%)	11(69%)	21	16(76%)	10(63%)	6(37%)
S0	13	9(69%)	2(22%)	7(78%)	13	8(62%)	5(63%)	3(37%)
Sa	10	4(40%)	1(25%)	3(75%)	10	3(30%)	1(33%)	2(67%)
Sb	21	7(33%)	2(29%)	5(71%)	21	9(43%)	5(56%)	4(44%)
Sc	11	0(0%)	0(0%)	0(0%)	11	0(0%)	0(0%)	0(0%)
Sm	2	0(0%)	0(0%)	0(0%)	2	0(0%)	0(0%)	0(0%)
Total	78	36(46%)	10(28%)	26(72%)	78	36(46%)	21(58%)	15(42%)

**Table 6.** Incidence type of nuclear activity for different morphologies from [S II] and [O I] diagnostic diagrams for (S+S) sample.

M.T.	[S II] Diagram				[O I] Diagram			
	Total	AGN	Seyfert	LINER	Total	AGN	Seyfert	LINER
Sa	60	29(48%)	7(24%)	22(76%)	60	31(52%)	18(58%)	13(42%)
Sb	92	30(33%)	13(43%)	17(57%)	92	23(25%)	10(43%)	13(57%)
Sc	39	5(13%)	4(80%)	1(20%)	39	2(5%)	2(100%)	0(0%)
Sm	12	1(8%)	1(100%)	0(0%)	12	0(0%)	0(0%)	0(0%)
Total	203	69(34%)	29(42%)	40(58%)	203	56(28%)	30(54%)	26(46%)

of type of interaction) for the total sample and for objects with masses  $10^{10.0}M_{\odot}$  and  $10^{10.5}M_{\odot}$ . For this plot, only objects with emission lines are considered, and to avoid small number statistics, all spirals have been grouped as Late type objects, while E and S0 have been grouped as early type. It is clear from this Figure, that any differences in AGN fraction for late type objects are of the 10% (similar to the error), and that early type objects show strikingly the same fraction independently of the environment and type of interaction. In fact, from this plot it is clear that early type galaxies showing emission lines are almost all AGN, and this fraction decreases towards later types. We note however, that when galaxies without emission lines are considered, early type galaxies show a lower fraction of AGN when compared to later types (as found for the entire sample), even at high masses.

The most striking result in our analysis is that in all the 385 revised spectra, only 4 objects present AGN type 1 activity, which represents  $\sim 1\%$  of the sample. This result does not seem to support the unified model at least in its simpler version.

#### 4 DISCUSSION

We have made a comparison of the incidence of nuclear activity in a sample of paired galaxies with the incidence in a sample of isolated galaxies. All our samples were analyzed in a homogeneous and consistent way. This comparison has been done separating according to morphological types and stellar masses.

Our results confirm that there is a link between morphology and nuclear activity. When galaxies with and without emission lines are considered (the entire samples), early type spirals host the larger fractions of AGN. The incidence of activity shows a growing distribution from E to Sb morphological types, decreasing sharply for later types. When

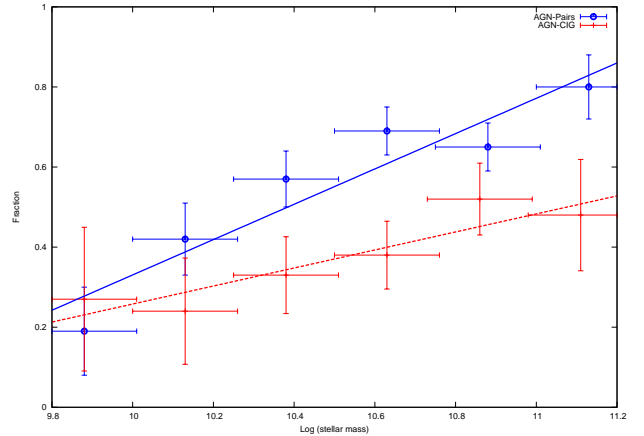


**Figure 10.** Comparison between fraction of AGN in pairs and AGN isolated galaxies as function of stellar mass. AGN in pairs are represented by (blue) filled circles and AGN isolated objects by (red) crosses. Errors in the y-direction are the standard deviation per bin and errors in x-direction simply denote the full range of mass in each bin. A different slope is remarkable above  $10^{10}$  solar masses between AGN in pairs and AGN in isolated systems. However, such slope might be the result of the different morphological mixes in both samples.

only galaxies with emission lines are considered, the incidence of AGN activity in Elliptical and Spheroidal galaxies is particularly large (around  $\sim 75\%$ , almost all LINERs). This incidence is similar in both isolated and paired galaxies. This means that if an early type galaxy shows emission lines, it is very likely that it hosts nuclear activity. For spiral galaxies with emission lines (both paired and isolated), the incidence of AGN activity (versus star forming objects) decreases gradually from early to late type galaxies, in other words, as the size of the bulge decreases. Similar results

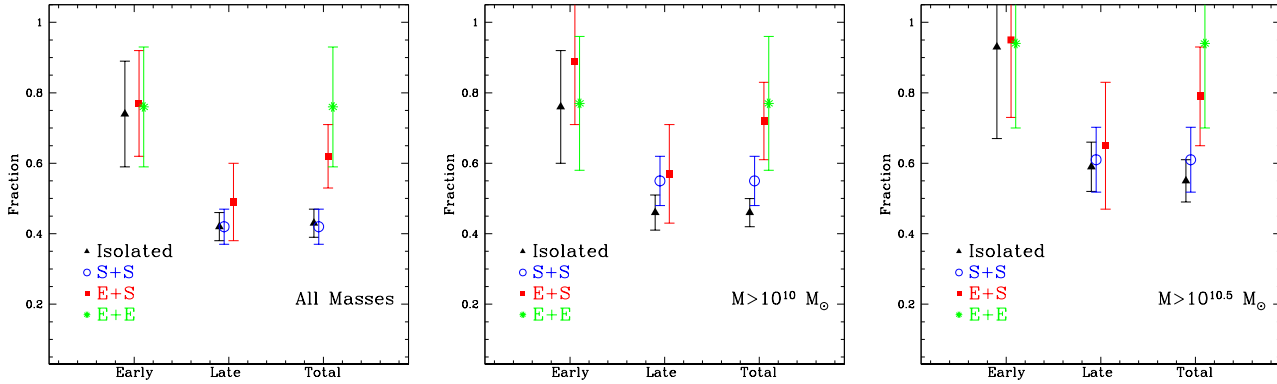


**Figure 11.** Fraction of AGN, considering only galaxies with emission lines, in the different type of pairs and in isolated galaxies as a function of morphological type for three different ranges of mass: (Left) All galaxies; (Center) Galaxies with mass  $> 10^{10} M_{\odot}$ ; and (Right) Galaxies with mass  $> 10^{10.5} M_{\odot}$ . No significant excess of AGN in interacting galaxies is observed when galaxies with similar masses and morphologies are considered.

have been found by Varela et al. (2004); Coziol et al. (2011); Sabater et al. (2012); Hernandez-Ibarra et al. (2012).

The fraction of AGN in spirals can be readily understood considering that both the presence of a dominant bulge and a large reservoir of gas are required to canalize gas and feed a supermassive black hole (SMBH). The large fraction of AGN in Ellipticals when only emission line objects are taken into account may be explained from the fact that, when these galaxies have some supply of gas (either its own, or accreted from the companion), it can reach the inner regions easily and feed the SMBH (rather than stop in the way to the center and produce star formation). When non-emission line galaxies are also considered, the fraction of AGN in early types decreases significantly, since there is a larger number of non-emitting sources in this samples, considering that in early galaxies there is negligible ongoing star formation. The fraction of Seyfert nuclei increases from early to late types. Only  $\sim 4\%$  of the galaxies in ( $E+E$ ) pairs host a Seyfert nuclei ( $\sim 12\%$  of the AGN in ( $E+E$ ) pairs). However, the fraction of Seyfert nuclei rises to  $\sim 10\%$  in ( $E+S$ ) pairs ( $\sim 28\%$  of the AGN in this kind of pairs), and to  $\sim 14\%$  in ( $S+S$ ) systems ( $\sim 42\%$  of the AGN in ( $s+S$ ) pairs). These trends may result from the limited supply of material in early type objects.

A striking and surprising result is that isolated and paired galaxies yield similar levels of nuclear activity incidence, with only marginal indication for an enhancement in interacting, late type objects. The lack of differences appears to be independent of mass. This suggests that this type of relatively weak (i.e. tidal) interaction between low luminosity galaxies is not a dominant triggering force of nuclear activity, at least, for low luminosity AGN (LLAGN), as the ones found in the pairs of galaxies and in isolated objects. Although there is clear evidence that more luminous AGN can be triggered by interactions (see §1), the latter are clearly not a sufficient condition for the onset of a SMBH. Perhaps, stronger gravitational interactions (such as a very close encounter and of course mergers) are needed for gravitational triggering of activity.

Interactions are not a necessary condition either for the existence of these LLAGN, since the fraction of isolated

galaxies hosting such a nucleus is large and comparable to pairs of galaxies. Taken at face value, our results indicate that, although non-axisymmetric perturbations (such as bars or interactions) are important in AGN triggering, the exact necessary and sufficient processes to form an active galaxy (either of high or low luminosity) remain a mystery. Overall, these results indicate that secular evolution processes (see H-I13) can trigger/maintain low luminosity AGN activity, and as such might be important in some processes of the galaxy. However, as discussed by H-I13, AGN with such low luminosities and accretion rates ( $0.001 - 10^{-5} M_{\odot}/\text{yr}$ ) galaxies cannot grow their central black holes through these low-level activity, nor can they evolve from one type of object to another.

Perhaps, the more relevant result from this work is the fact that out of the 150 AGN galaxies in pairs, only 4 have (albeit a small) broad component: We find one 1.9 Sy, two 1.8 Sy and one 1.5 Sy. Not even one type 1 Sy. This result is at odds with the simplest formulation of the unified model (UM) (Antonucci 1993), which takes into account orientation and obscuration effects only. An evolutionary scheme, on the other hand, may explain this result. A Seyfert 1 may require as much as 1 Gyr after an interaction to appear (Krongold et al. 2002). In this case, an interaction may trigger first a circumnuclear starburst, and subsequently non-thermal nuclear activity. Such scheme could explain the lack of type 1 nucleus in these pairs of galaxies, considering that there has not been enough time for the Sy 1 nucleus to appear. However, the lack of enhancement in the fraction of AGN in the pairs of galaxies, when compared to isolated objects, would require that we are seeing these pairs on its initial approach. Whether this is the case or not, our results are consistent with the idea that the BLR in active galaxies can only be formed at higher luminosities/accretion rates (e.g. Nicastro 2000, Elitzur & Ho 2009).

**Table 7.** Incidence of nuclear activity for the different morphological types as a function of pair morphology derived from [N II] BPT diagnostic diagram.

Fraction of AGN (including composite objects) in Early Type Galaxies								
M.T.	Galaxies with Emission lines				Total sample			
	E+E	E+S	S+S	Isolated	E+E	E+S	S+S	Isolated
E	13/18 (72%)	16/21 (76%)	–	10/14 (71%)	13/41 (32%)	16/33 (48%)	–	10/23 (43%)
S0	5/7 (71%)	10/13 (77%)	–	21/30 (70%)	5/14 (36%)	10/19 (53%)	–	21/38 (55%)
Total	18/25 (72%)	26/34 (76%)	–	31/44 (70%)	18/55 (33%)	26/52 (50%)	–	31/61 (51%)

Fraction of AGN (including composite objects) in Late Type Galaxies								
M.T.	Galaxies with Emission lines				Total sample			
	E+E	E+S	S+S	Isolated	E+E	E+S	S+S	Isolated
Sa	–	6/10 (60%)	36/60 (60%)	25/38 (66%)	–	6/13 (46%)	36/65 (55%)	25/38 (66%)
Sb	–	13/21 (62%)	38/92 (41%)	55/122 (45%)	–	13/21 (62%)	38/97 (39%)	55/124 (44%)
Sc	–	3/11 (27%)	6/39 (15%)	37/124 (30%)	–	3/11 (27%)	6/40 (39%)	37/124 (30%)
Sm	–	0/2 (0%)	1/12 (8%)	2/20 (10%)	–	0/2 (0%)	1/12 (8%)	2/20 (10%)
Total	–	22/44 (50%)	81/203 (40%)	119/304 (39%)	–	22/47 (47%)	81/214 (38%)	119/306 (39%)

Fraction of AGN (including composite objects) in the Pair Samples								
Total	Galaxies with Emission lines				Total sample			
	E+E	E+S	S+S	Isolated	E+E	E+S	S+S	Isolated
Total	18/25 (72%)	48/78 (62%)	81/203 (40%)	150/348 (43%)	18/55 (33%)	48/99 (48%)	81/214 (38%)	150/367 (41%)

Total Fraction of AGN in Pairs vs. Isolated Samples				
Total	Galaxies with Emission lines		Total sample	
	Galaxies in Pairs	Isolated Galaxies	Galaxies in Pairs	Isolated Galaxies
Total	147/306(48%)	150/348 (43%)	147/368(40%)	150/367 (41%)

## ACKNOWLEDGMENTS

FJHI acknowledges a graduate student scholarship from CONACYT. DD acknowledge support from grant IN111610 PAPIIT, UNAM.

## REFERENCES

Abazajian K. N. et al., 2009, *ApJS*, 182, 543  
Antonucci R., 1993, *Ann. Rev. Ast. & Ast.*, 31, 473  
Baldwin J. A., Phillips M. M., Terlevich R., 1981, *Publications of the ASP*, 93, 5  
Barnes J. E., Hernquist L., 1992, *Ann. Rev. Ast. & Ast.*, 30, 705  
Bitsakis T., Dultzin D., Ciesla L., Krongold Y., Charmandaris V., Zezas A., 2015, *MNRAS*, 450, 3114  
Bell E. F., McIntosh D. H., Katz N., Weinberg M. D., 2003, *ApJS*, 149, 289  
Coziol R., Torres-Papaqui J. P., Plauchu-Frayn I., Islas-Islas J. M., Ortega-Minakata R. A., Neri-Larios D. M., Andernach H., 2011, *Revista Mexicana de Astronomía y Astrofísica*, 47, 361  
Cox T. J., Jonsson P., Somerville R. S., Primack J. R., Dekel A., 2008, *MNRAS*, 384, 386  
Dahari O., 1985, *ApJS*, 57, 643  
Dahari O. A., 1984, PhD thesis, California Univ., Santa Cruz.  
de Mello D. F., Keel W. C., Sulentic J. W., Rampazzo R., 1995, in van der Kruit P. C., Gilmore G., eds, *IAU Symposium Vol. 164, Stellar Populations*. p. 434  
de Mello D. F., Sulentic J. W., de Souza R. E., Reduzzi L., Rampazzo R., 1996, *Astronomy and Astrophysics*, 308, 387  
Domingue D. L., Sulentic J. W., Durbala A., 2005, *Astronomical Journal*, 129, 2579  
Dultzin D. et al., 2008, *ArXiv e-prints*

Dultzin-Hacyan D., Krongold Y., Fuentes-Guridi I., Marziani P., 1999, *ApJL*, 513, L111  
Elitzur M., Ho L. C., 2009, *ApJ*, 701, L91  
Ellison S. L., Patton D. R., Simard L., McConnachie A. W., 2008, *AJ*, 135, 1877  
Ellison S. L., Patton D. R., Mendel J. T., Scudder J. M., 2011, *MNRAS*, 418, 2043  
Franco-Balderas A., Hernández-Toledo H. M., Dultzin-Hacyan D., 2004, *Astronomy and Astrophysics*, 417, 411  
González-Martín O., Masegosa J., Márquez I., Jiménez-Bailón E., 2007, in Karas V., Matt G., eds, *IAU Symposium Vol. 238, IAU Symposium*. pp 373–374  
González-Martín O., et al., 2015, *arXiv*, arXiv:1501.03826  
Hao L. et al., 2005, *Astronomical Journal*, 129, 1795  
Hernandez-Ibarra F., Dultzin D., Krongold Y., Del Olmo A., Perea J., Gonzalez J., 2012, *arXiv*, arXiv:1206.6777  
Hernández-Ibarra F. J., Dultzin D., Krongold Y., Olmo A. d., Perea J., González J., 2013, *MNRAS*, 434, 336  
Hernández Toledo H. M., Dultzin-Hacyan D., Gonzalez J. J., Sulentic J. W., 1999, *Astronomical Journal*, 118, 108  
Hopkins P. F., Hernquist L., Martini P., Cox T. J., Robertson B., Di Matteo T., Springel V., 2005, *ApJ*, 625, L71  
Karachentsev I. D., 1972, *Soobshcheniya Spetsial'noj Astrofizicheskoy Observatorii*, 7, 1  
Kauffmann G. et al., 2003, *MNRAS*, 346, 1055  
Keel W. C., 1993, *Astronomical Journal*, 106, 1771  
Kennicutt Jr. R. C., Keel W. C., 1984, *ApJL*, 279, L5  
Kewley L. J., Dopita M. A., Sutherland R. S., Heisler C. A., Trevena J., 2001, *ApJ*, 556, 121  
Kewley L. J., Groves B., Kauffmann G., Heckman T., 2006, *MNRAS*, 372, 961  
Knapen J. H., James P. A., 2009, *ApJ*, 698, 1437  
Koulouridis E., Chavushyan V., Plionis M., Krongold Y., Dultzin-Hacyan D., 2006, *ApJ*, 651, 93  
Koulouridis E., Plionis M., Chavushyan V., Dultzin-

- Hacyan D., Krongold Y., Goudis C., 2006, *ApJ*, 639, 37
- Koulouridis E., Plionis M., Chavushyan V., Dultzin D., Krongold Y., Georgantopoulos I., León-Tavares J., 2013, *A&A*, 552, A135
- Krongold Y., Dultzin-Hacyan D., Marziani P., 2001, *Astronomical Journal*, 121, 702
- Krongold Y., Dultzin-Hacyan D., Marziani P., 2002, 572, 169
- Krongold Y., Dultzin-Hacyan D., Marziani P., 2003, in Collin S., Combes F., Shlosman I., eds, *Astronomical Society of the Pacific Conference Series Vol. 290, Active Galactic Nuclei: From Central Engine to Host Galaxy*. p. 523
- Lintott C. J., et al., 2008, *MNRAS*, 389, 1179
- Liu, X., Shen, Y., Strauss, M. A. 2012. Active Galactic Nucleus Pairs from the Sloan Digital Sky Survey. II. Evidence for Tidally Enhanced Star Formation and Black Hole Accretion. *The Astrophysical Journal* 745, 94.
- Márquez I., Masegosa J., 2008, in *Revista Mexicana de Astronomía y Astrofísica Conference Series*. pp 150–154
- Martínez M. A., del Olmo A., Coziol R., Focardi P., 2008, *ApJ*, 678, L9
- Martínez M. A., Del Olmo A., Coziol R., Perea J., 2010, *AJ*, 139, 1199
- Martini P., et al., 2013, *ApJ*, 768, 1
- Martini P., Mulchaey J. S., Kelson D. D., 2007, *ApJ*, 664, 761
- Mendoza-Castrejón S., Dultzin D., Krongold Y., González J. J., Elitzur M., 2015, *MNRAS*, 447, 2437
- Nair P. B., Abraham R. G., 2010, *yCat*, 218, 60427
- Nicastro F., 2000, *ApJ*, 530, L65
- Perry J. J., Dyson J. E., 1985, *MNRAS*, 213, 665
- Popesso P., Biviano A., 2006, *A&A*, 460, L23
- Rogers B., Ferreras I., Kaviraj S., Pasquali A., Sarzi M., 2009, *MNRAS*, 399, 2172
- Sabater J., Verdes-Montenegro L., Leon S., Best P., Sulentic J., 2012, *Astronomy and Astrophysics*, 545, A15
- Schmitt H. R., 2001, *Astronomical Journal*, 122, 2243
- Sorrentino G., Radovich M., Rifatto A., 2006, *Astronomy and Astrophysics*, 451, 809
- Springel V., Di Matteo T., Hernquist L., 2005, *ApJ*, 620, L79
- Stauffer J. R., 1982a, *ApJ*, 262, 66
- Stauffer J. R., 1982b, *ApJS*, 50, 517
- Storchi-Bergmann T., 2008, in *Revista Mexicana de Astronomía y Astrofísica Conference Series*. pp 139–146
- Trouille L., Barger A. J., Tremonti C., 2011, *ApJ*, 742, 46
- Varela J., Moles M., Márquez I., Galletta G., Masegosa J., Bettoni D., 2004, *A&A*, 420, 873
- Veilleux S., Osterbrock D. E., 1987, *ApJS*, 63, 295
- Verdes-Montenegro L., Yun M. S., Williams B. A., Huchtmeier W. K., Del Olmo A., Perea J., 2001, *A&A*, 377, 812
- Villarroel B., Korn A. J., 2014, *NatPh*, 10, 417
- Villforth C., Sarajedini V., Koekemoer A., 2012, *MNRAS*, 426, 360
- Winkler H., 1992, *MNRAS*, 257, 677

Table A1. Logarithm intensities ratios and their errors for (E+E) sample.

Object	M.T. <sup>a</sup>	LOG([N II]/H $\alpha$ )	LOG([O III]/H $\beta$ )	LOG([S II]/H $\alpha$ )	LOG([O I]/H $\alpha$ )	Type
Elliptical						
KPG145B	E	0.1852 $\pm$ 0.0233	0.1772 $\pm$ 0.0714	0.2792 $\pm$ 0.0292	-0.7272 $\pm$ 0.0758	LINER
KPG170B	E	0.1994 $\pm$ 0.0698	0.0503 $\pm$ 0.1249	0.2482 $\pm$ 0.0792	-0.8132 $\pm$ 0.2803	LINER
KPG192B	E	0.3005 $\pm$ 0.0333	0.2032 $\pm$ 0.1058	0.2222 $\pm$ 0.0445	-0.4733 $\pm$ 0.0740	LINER
KPG204A	E	-0.6887 $\pm$ 0.0087	-0.2983 $\pm$ 0.0685	-0.5590 $\pm$ 0.0159	-1.6857 $\pm$ 0.0682	Star-forming
KPG223A	E	0.3833 $\pm$ 0.0353	-0.0495 $\pm$ 0.0947	0.1936 $\pm$ 0.0389	-0.5300 $\pm$ 0.0684	LINER
KPG235B	E	0.2970 $\pm$ 0.0240	-0.0619 $\pm$ 0.0803	-0.1959 $\pm$ 0.0396	-1.1057 $\pm$ 0.1250	Sy2
KPG238A	E	-0.0985 $\pm$ 0.0713	-0.1181 $\pm$ 0.1809	-0.3106 $\pm$ 0.1496	-1.3532 $\pm$ 0.6396	AGN
KPG238B	E	-0.2778 $\pm$ 0.0091	0.1318 $\pm$ 0.0065	-1.0212 $\pm$ 0.0210	-1.3708 $\pm$ 0.0233	AGN*
KPG361B	E	0.1256 $\pm$ 0.0889	0.1128 $\pm$ 0.2682	0.0330 $\pm$ 0.1426	-1.0029 $\pm$ 0.5114	S-L
KPG372B	E	-0.0923 $\pm$ 0.0071	-0.4935 $\pm$ 0.0085	-0.3473 $\pm$ 0.0071	-1.6329 $\pm$ 0.0191	Star-forming
KPG373A	E	0.5639 $\pm$ 0.0450	0.2682 $\pm$ 0.1039	0.1240 $\pm$ 0.0695	-0.6585 $\pm$ 0.1421	S-L
KPG399A	E	0.6728 $\pm$ 0.0459	0.3764 $\pm$ 0.2281	0.2738 $\pm$ 0.0657	-0.6724 $\pm$ 0.1656	S-L
KPG454A	E	-0.7423 $\pm$ 0.0065	-0.4240 $\pm$ 0.0199	-0.4600 $\pm$ 0.0078	-1.8731 $\pm$ 0.0401	Star-forming
KPG454B	E	-0.1145 $\pm$ 0.0110	-0.4070 $\pm$ 0.0196	-0.3490 $\pm$ 0.0133	-1.7599 $\pm$ 0.0843	Star-forming
KPG489A	E	-0.3270 $\pm$ 0.2184	0.1827 $\pm$ 0.2343	0.3003 $\pm$ 0.2657	-0.1871 $\pm$ 0.3307	LINER
KPG489B	E	-0.0934 $\pm$ 0.0477	-0.0634 $\pm$ 0.1344	-0.0082 $\pm$ 0.0654	-1.5781 $\pm$ 0.7487	AGN
KPG510B	E	0.1006 $\pm$ 0.0070	0.9620 $\pm$ 0.0095	-0.2733 $\pm$ 0.0095	-1.0261 $\pm$ 0.0205	Sy1.8
KPG600B	E	-0.1817 $\pm$ 0.0169	-0.4024 $\pm$ 0.0415	-0.2919 $\pm$ 0.0217	-1.5216 $\pm$ 0.1035	Star-forming
Spheroidal						
KPG184B	S0	0.4740 $\pm$ 0.0313	0.3984 $\pm$ 0.1213	0.2363 $\pm$ 0.0469	-0.6619 $\pm$ 0.1102	LINER
KPG208A	S0	0.4751 $\pm$ 0.0102	-0.3961 $\pm$ 0.0124	-0.1139 $\pm$ 0.0107	-0.5039 $\pm$ 0.0093	Sy1.5
KPG208B	S0	-0.1639 $\pm$ 0.0068	-0.6217 $\pm$ 0.0095	-0.4434 $\pm$ 0.0073	-1.8897 $\pm$ 0.0319	Star-forming
KPG277B	SB0	0.1127 $\pm$ 0.0388	0.2444 $\pm$ 0.1296	0.1511 $\pm$ 0.0584	-0.8281 $\pm$ 0.1667	LINER
KPG359A	SB0	0.4238 $\pm$ 0.0893	-0.2928 $\pm$ 0.2166	0.0869 $\pm$ 0.0805	-0.7440 $\pm$ 0.1854	S-L
KPG431B	S0	-0.4124 $\pm$ 0.0725	0.1635 $\pm$ 0.3280	0.3248 $\pm$ 0.0841	-1.8051 $\pm$ 2.5943	AGN
KPG492A	S0	1.6559 $\pm$ 0.0812	0.4975 $\pm$ -	0.5138 $\pm$ 0.0994	-0.3183 $\pm$ 0.1803	S-L

<sup>a</sup>M.T.- Morphological Type.

\*AGN classification denotes those galaxies that are AGN according to the [N II] diagrams but not to the [S II] and/or [O I].

†L-S classification means that galaxies fall in the separation line for Seyfert and LINER according to [S II] and [O I] diagrams.

\*Type with weak broad component in permitted lines. Seyfert quantitative classification according to Winkler (1992).

## APPENDIX A: SAMPLES OF (E+E), (E+S), AND (S+S) PAIRS

Tables A1, A2, and A3 present the samples for the different types of pairs.

Table A2. Logarithm intensities ratios and their errors for (E+S) sample.

Object	M.T. <sup>a</sup>	LOG([N II]/H $\alpha$ )	LOG([O III]/H $\beta$ )	LOG([S II]/H $\alpha$ )	LOG([O I]/H $\alpha$ )	Type
Elliptical						
KPG055A	E	0.4993 $\pm$ 0.1027	1.0842 $\pm$ 0.8013	0.4597 $\pm$ 0.1329	-0.9006 $\pm$ 0.9222	S-L
KPG089B	E	0.3029 $\pm$ 0.0896	0.7262 $\pm$ 0.4881	0.0451 $\pm$ 0.1716	-0.4415 $\pm$ 0.2174	S-L
KPG091B	E	0.4149 $\pm$ 0.0881	0.1889 $\pm$ 0.1558	0.3686 $\pm$ 0.1197	-1.0699 $\pm$ 1.2131	AGN
KPG144B	E	-0.4333 $\pm$ 0.0086	-0.7456 $\pm$ 0.0294	-0.5566 $\pm$ 0.0130	-1.8652 $\pm$ 0.0627	Star-forming
KPG155A	E	-0.6479 $\pm$ 0.0128	0.0830 $\pm$ 0.0188	-0.4416 $\pm$ 0.0158	-1.3675 $\pm$ 0.0876	Star-forming
KPG167A	E	0.3963 $\pm$ 0.0562	0.2965 $\pm$ 0.1364	0.2132 $\pm$ 0.0893	-0.7086 $\pm$ 0.2628	LINER
KPG197B	E	0.1071 $\pm$ 0.1254	0.5876 $\pm$ 0.5488	-0.0212 $\pm$ 0.2225	-1.3599 $\pm$ 1.8493	AGN
KPG198B	E	0.2118 $\pm$ 0.0666	0.4295 $\pm$ 0.1479	0.1489 $\pm$ 0.0988	-1.0428 $\pm$ 0.73956	AGN
KPG244A	E	0.2472 $\pm$ 0.1071	0.9321 $\pm$ 0.5472	0.0682 $\pm$ 0.1872	-0.3952 $\pm$ 0.2798	S-L
KPG254B	E	0.1830 $\pm$ 0.1103	0.7963 $\pm$ 0.6008	0.1519 $\pm$ 0.1599	-0.5364 $\pm$ 0.3098	S-L
KPG260B	E	-0.0098 $\pm$ 0.0491	0.5369 $\pm$ 0.1214	-0.0516 $\pm$ 0.0798	-0.7262 $\pm$ 0.1743	S-L
KPG339B	E	0.3400 $\pm$ 0.1271	0.4900 $\pm$ 0.2531	-0.4000 $\pm$ 0.5529	-0.6500 $\pm$ 0.7326	S-L
KPG363A	E	-0.1500 $\pm$ 0.0048	0.3900 $\pm$ 0.0100	-0.2062 $\pm$ 0.0053	-1.1900 $\pm$ 0.0286	Sy2
KPG383A	E	-0.0589 $\pm$ 0.0253	0.1041 $\pm$ 0.0549	0.0646 $\pm$ 0.0323	-0.6045 $\pm$ 0.0432	LINER
KPG394A	E	-0.5482 $\pm$ 0.0103	-0.3162 $\pm$ 0.0199	-0.4843 $\pm$ 0.0135	-1.7759 $\pm$ 0.1200	Star-forming
KPG412B	E	0.0100 $\pm$ 0.0861	0.3000 $\pm$ 0.5584	-0.3400 $\pm$ 0.2379	-0.5900 $\pm$ 0.1510	AGN
KPG414B	E	-1.0658 $\pm$ 0.0064	0.5854 $\pm$ 0.0050	-0.8526 $\pm$ 0.0075	-1.9263 $\pm$ 0.3964	Star-forming
KPG432A	E/S0	0.1500 $\pm$ 0.1628	0.6500 $\pm$ 0.2518	-0.0800 $\pm$ 0.3282	-0.79 $\pm$ 1.3913	AGN
KPG466B	E/S0	-0.2432 $\pm$ 0.0054	-0.5659 $\pm$ 0.0156	-0.5076 $\pm$ 0.0082	-1.4698 $\pm$ 0.0223	AGN
KPG494B	E	-0.5027 $\pm$ 0.0065	0.0234 $\pm$ 0.0087	-0.6204 $\pm$ 0.0094	-1.7156 $\pm$ 0.1363	Star-forming
KPG565A	E	0.0575 $\pm$ 0.1217	0.3907 $\pm$ 0.1637	0.1120 $\pm$ 0.1654	-1.0119 $\pm$ 0.6625	S-L
Spheroidal						
KPG006A	S0	-0.4195 $\pm$ 0.0048	-0.7951 $\pm$ 0.0234	-0.6294 $\pm$ 0.0084	-1.7974 $\pm$ 0.0364	Star-forming
KPG062A	S0/a	0.2940 $\pm$ 0.0327	0.6557 $\pm$ 0.1096	0.1072 $\pm$ 0.0540	-0.4205 $\pm$ 0.0758	LINER
KPG162A	S0	0.0361 $\pm$ 0.0650	0.3679 $\pm$ 0.1335	0.1669 $\pm$ 0.0810	-0.5131 $\pm$ 0.1451	LINER
KPG231A	S0	-0.1258 $\pm$ 0.0148	-0.1432 $\pm$ 0.0520	-0.3094 $\pm$ 0.0275	-1.1732 $\pm$ 0.0599	AGN
KPG243B	S0	-0.2481 $\pm$ 0.0124	-0.2337 $\pm$ 0.0358	-0.4167 $\pm$ 0.0220	-1.2459 $\pm$ 0.0583	AGN
KPG269A	S0	-0.3083 $\pm$ 0.0240	-0.0619 $\pm$ 0.0434	-0.1174 $\pm$ 0.0289	-0.6155 $\pm$ 0.0305	LINER
KPG275B	S0	-0.3729 $\pm$ 0.0071	-0.6161 $\pm$ 0.0192	-0.5494 $\pm$ 0.0106	-1.7735 $\pm$ 0.0488	Star-forming
KPG304A	S0	-0.0882 $\pm$ 0.0262	0.0342 $\pm$ 0.1529	-0.2112 $\pm$ 0.0514	-1.5169 $\pm$ 0.3948	AGN
KPG317B	S0	-0.1411 $\pm$ 0.0318	-0.0846 $\pm$ 0.0741	-0.1459 $\pm$ 0.0495	-1.1398 $\pm$ 0.1709	AGN
KPG345B	S0/a	0.1580 $\pm$ 0.0438	0.4055 $\pm$ 0.2242	-0.1401 $\pm$ 0.0953	-1.0692 $\pm$ 0.2704	S-L
KPG374A	S0	0.2022 $\pm$ 0.0470	0.8882 $\pm$ 0.1197	0.2350 $\pm$ 0.0630	-0.5566 $\pm$ 0.2465	S-L
KPG392A	S0	0.2696 $\pm$ 0.0880	1.0135 $\pm$ 0.6311	0.1277 $\pm$ 0.1462	-0.6750 $\pm$ 0.4153	S-L
KPG402B	S0	-0.0239 $\pm$ 0.0353	0.3299 $\pm$ 0.0950	-0.0300 $\pm$ 0.0542	-1.2199 $\pm$ 0.3090	AGN
KPG408A	S0	0.0200 $\pm$ 0.0732	0.6000 $\pm$ -0.2100	-0.2200 $\pm$ 0.1651	-0.9400 $\pm$ 0.4780	S-L
KPG436A	S0	-0.4464 $\pm$ 0.0115	-0.8387 $\pm$ 0.0711	-0.6157 $\pm$ 0.0222	-0.9604 $\pm$ 0.2130	Star-forming
Sa						
KPG055B	Sa	-0.4164 $\pm$ 0.0355	-0.7504 $\pm$ 0.2962	-0.8892 $\pm$ 0.1335	-1.6462 $\pm$ 0.3224	Star-forming
KPG188A	Sa	-0.3864 $\pm$ 0.0080	-0.6397 $\pm$ 0.0235	-0.5991 $\pm$ 0.0130	-2.0507 $\pm$ 0.1187	Star-forming
KPG197A	Sa	0.3868 $\pm$ 0.1200	0.0900 $\pm$ 0.1292	0.3765 $\pm$ 0.1596	-0.8110 $\pm$ 1.1059	AGN
KPG199B	Sa	-0.3736 $\pm$ 0.0231	-0.4916 $\pm$ 0.1184	-0.4074 $\pm$ 0.0370	-1.6238 $\pm$ 0.2468	Star-forming
KPG239B	Sa	0.2471 $\pm$ 0.0812	-0.0440 $\pm$ 0.1153	0.1137 $\pm$ 0.1344	-0.6385 $\pm$ 0.3831	LINER
KPG260A	Sa	0.2989 $\pm$ 0.0445	0.2197 $\pm$ 0.0947	0.2112 $\pm$ 0.0657	-0.6162 $\pm$ 0.1726	LINER
KPG284A	Sa	-0.0451 $\pm$ 0.0223	-0.0490 $\pm$ 0.0966	-0.2627 $\pm$ 0.0448	-1.1747 $\pm$ 0.1157	AGN
KPG303B	Sa	0.2100 $\pm$ 0.1207	0.7600 $\pm$ -0.6208	-0.2500 $\pm$ 0.3488	-0.8100 $\pm$ 0.6206	Sy2
KPG317A	Sab	0.0313 $\pm$ 0.0566	0.0050 $\pm$ -0.2062	-0.6094 $\pm$ 0.2568	-0.8377 $\pm$ 0.2280	AGN
KPG402A	Sab	-0.5588 $\pm$ 0.0195	-0.0488 $\pm$ 0.0470	-0.3656 $\pm$ 0.0251	-1.3444 $\pm$ 0.0987	Star-forming
KPG439B	Sa	-0.2339 $\pm$ 0.0068	-0.3203 $\pm$ 0.0247	-0.5447 $\pm$ 0.0126	-2.0767 $\pm$ 0.0270	AGN
KPG548A	Sa	0.1074 $\pm$ 0.0315	0.3850 $\pm$ 0.0636	0.1196 $\pm$ 0.0437	-1.7587 $\pm$ 0.0811	AGN
KPG466A	Sa	-0.6200 $\pm$ 0.0098	0.6000 $\pm$ -0.2100	-0.1500 $\pm$ 0.0122	-0.6300 $\pm$ 0.0300	S-L
Sb						
KPG089A	Sb	-0.4280 $\pm$ 0.0063	-0.3958 $\pm$ 0.0129	-0.5371 $\pm$ 0.0090	-1.7760 $\pm$ 0.0579	Star-forming
KPG148A	Sb	-0.7930 $\pm$ 0.0076	0.1195 $\pm$ 0.0094	-0.6847 $\pm$ 0.0094	-1.9934 $\pm$ 0.1879	Star-forming
KPG162B	Sb	-0.2290 $\pm$ 0.0278	-0.1913 $\pm$ 0.0809	-0.3094 $\pm$ 0.0494	-1.7259 $\pm$ 0.4955	AGN
KPG202B	Sb	0.3768 $\pm$ 0.0374	1.0828 $\pm$ 0.2444	0.2005 $\pm$ 0.0582	-0.5370 $\pm$ 0.1209	S-L
KPG229B	Sb	-0.4275 $\pm$ 0.0133	-0.5682 $\pm$ 0.0579	-0.6502 $\pm$ 0.0274	-1.7358 $\pm$ 0.1053	Star-forming

Table A2 (cont'd)

Object	M.T. <sup>a</sup>	LOG([N II]/H $\alpha$ )	LOG([O III]/H $\beta$ )	LOG([S II]/H $\alpha$ )	LOG([O I]/H $\alpha$ )	Type
KPG243A	Sb	-0.2517 $\pm$ 0.0125	0.9063 $\pm$ 0.0179	-0.3040 $\pm$ 0.0191	-1.2366 $\pm$ 0.2450	Sy2
KPG248B	Sb	-0.0132 $\pm$ 0.0176	0.2765 $\pm$ 0.0935	-0.2094 $\pm$ 0.0349	-1.0981 $\pm$ 0.1070	S-L
KPG254A	Sbab	0.1189 $\pm$ 0.0062	1.0848 $\pm$ 0.0092	-0.2198 $\pm$ 0.0098	-0.7999 $\pm$ 0.0984	Sy2
KPG269B	Sb	-0.5115 $\pm$ 0.0073	-0.3156 $\pm$ 0.0140	-0.5588 $\pm$ 0.0101	-1.7537 $\pm$ 0.0710	Star-forming
KPG339A	Sb	-0.5009 $\pm$ 0.0144	-0.9664 $\pm$ 0.1302	-0.5756 $\pm$ 0.0244	-1.5262 $\pm$ 0.0801	Star-forming
KPG345A	Sbs(dm)	-0.6208 $\pm$ 0.0266	-0.1099 $\pm$ 0.0559	-0.2803 $\pm$ 0.0271	-1.1642 $\pm$ 0.1137	Star-forming
KPG374B	Sbc	-0.4636 $\pm$ 0.0162	-0.6559 $\pm$ 0.1089	-0.5556 $\pm$ 0.0298	-1.6522 $\pm$ 0.1230	Star-forming
KPG392B	Sb	-0.1453 $\pm$ 0.0412	0.3090 $\pm$ 0.0698	-0.1000 $\pm$ 0.0604	-0.9476 $\pm$ 0.2024	S-L
KPG408B	Sb	-0.5318 $\pm$ 0.0276	-0.0493 $\pm$ 0.0680	-0.2616 $\pm$ 0.0306	-1.2143 $\pm$ 0.1363	Star-forming
KPG416A	Sb	-0.4165 $\pm$ 0.0079	-0.7686 $\pm$ 0.0294	-0.6609 $\pm$ 0.0129	-2.0159 $\pm$ 0.0828	Star-forming
KPG419A	SBb	-0.0400 $\pm$ 0.0073	1.0000 $\pm$ -0.2100	-0.1400 $\pm$ 0.0082	-0.8800 $\pm$ 0.0654	Sy1.9
KPG432B	Sb	-0.5281 $\pm$ 0.0183	-0.8646 $\pm$ 0.1123	-0.5979 $\pm$ 0.0308	-0.8139 $\pm$ 0.6375	Star-forming
KPG436B	Sb	-0.3351 $\pm$ 0.0260	-0.2282 $\pm$ 0.1648	-0.5081 $\pm$ 0.0554	-2.3363 $\pm$ 0.1890	Star-forming
KPG484B	Sb	-0.4621 $\pm$ 0.0242	-0.5690 $\pm$ 0.1357	-0.6541 $\pm$ 0.0586	-1.3153 $\pm$ 0.5506	Star-forming
KPG494A	Sbc	-0.2737 $\pm$ 0.0106	-0.4524 $\pm$ 0.0416	-0.4959 $\pm$ 0.0207	-0.6307 $\pm$ 0.1096	AGN
KPG497B	Sb	0.2149 $\pm$ 0.0372	0.1282 $\pm$ 0.1041	0.2410 $\pm$ 0.0495	-1.9189 $\pm$ 0.2746	AGN
KPG558A	Sb	-0.3820 $\pm$ 0.0216	-0.5685 $\pm$ 0.1345	-0.5350 $\pm$ 0.0464	-1.8762 $\pm$ 2.0941	Star-forming
KPG565B	Sb	-0.5528 $\pm$ 0.0163	-0.2266 $\pm$ 0.0389	-0.4436 $\pm$ 0.0215	-0.5792 $\pm$ 0.1180	Star-forming
Sc						
KPG058A	Sc	-0.2334 $\pm$ 0.0200	-0.3081 $\pm$ 0.1289	-0.3386 $\pm$ 0.0395	-1.2968 $\pm$ 0.1063	AGN
KPG287A	Sc	-0.4494 $\pm$ 0.0290	-0.7093 $\pm$ 0.2075	-0.5882 $\pm$ 0.0640	-1.7455 $\pm$ 0.4297	Star-forming
KPG314B	Sc	-0.4574 $\pm$ 0.0225	-0.6110 $\pm$ 0.1444	-0.2951 $\pm$ 0.0290	-1.2424 $\pm$ 0.0949	Star-forming
KPG353A	Sc	-0.6103 $\pm$ 0.0155	-0.9310 $\pm$ 0.1019	-0.8004 $\pm$ 0.0309	-2.1018 $\pm$ 0.2166	Star-forming
KPG407A	Sc	-0.1260 $\pm$ 0.0093	0.1290 $\pm$ 0.0184	-0.4357 $\pm$ 0.0173	-1.3858 $\pm$ 0.0731	AGN
KPG412A	Sc	-0.3194 $\pm$ 0.0167	-0.2700 $\pm$ 0.0974	-0.4120 $\pm$ 0.0315	-1.3003 $\pm$ 0.0892	Star-forming
KPG464B	Sc	-0.3634 $\pm$ 0.0338	-0.6033 $\pm$ 0.2548	-0.6392 $\pm$ 0.0926	-1.4960 $\pm$ 0.1895	Star-forming
Sm						
KPG198A	Sm	-0.6659 $\pm$ 0.0053	0.0858 $\pm$ 0.0066	-0.6191 $\pm$ 0.0066	-1.6593 $\pm$ 0.0651	Star-forming
KPG414A	Sm	-0.7539 $\pm$ 0.0291	0.1398 $\pm$ 0.0340	-0.3100 $\pm$ 0.0247	-1.4477 $\pm$ 0.2577	Star-forming

<sup>a</sup>M.T.- Morphological Type.

†AGN classification denotes those galaxies that are AGN according to the [N II] diagrams but not to the [S II] and/or [O I].

‡L-S classification means that galaxies fall in the separation line for Seyfert and LINER according to [S II] and [O I] diagrams.

\*Type with weak broad component in permitted lines. Seyfert quantitative classification according to Winkler (1992).

Table A3. Logarithm intensities ratios and their errors for (S+S) sample.

Object	M.T. <sup>a</sup>	LOG([N II]/H $\alpha$ )	LOG([O III]/H $\beta$ )	LOG([S II]/H $\alpha$ )	LOG([O I]/H $\alpha$ )	Type
Sa						
KPG052B	SBa	-0.0227 $\pm$ 0.0390	0.3490 $\pm$ 0.0996	0.1075 $\pm$ 0.0491	-0.7634 $\pm$ 0.1161	LINER
KPG161A	Sa	-0.5634 $\pm$ 0.0375	0.0263 $\pm$ 0.0066	-0.5587 $\pm$ 0.0491	-1.6507 $\pm$ 0.0301	Star-forming
KPG174B	Sab	0.2549 $\pm$ 0.0612	0.2078 $\pm$ 0.0900	0.1152 $\pm$ 0.0763	-0.8191 $\pm$ 0.1435	LINER
KPG185B	Sab	-0.2759 $\pm$ 0.0069	-0.2778 $\pm$ 0.0168	-0.5190 $\pm$ 0.0130	-1.6973 $\pm$ 0.0616	AGN
KPG190B	Sab	0.1749 $\pm$ 0.0543	0.3164 $\pm$ 0.1391	0.0379 $\pm$ 0.0914	-0.7517 $\pm$ 0.2010	LINER
KPG201A	Sa	0.4490 $\pm$ 0.0698	1.4683 $\pm$ 1.8727	0.4423 $\pm$ 0.0912	-0.3428 $\pm$ 0.1627	S-L
KPG211A	Sa	0.4428 $\pm$ 0.0748	0.7200 $\pm$ 0.2252	0.1979 $\pm$ 0.1218	-0.5703 $\pm$ 0.1677	LINER
KPG213B	Sa	0.3444 $\pm$ 0.0579	0.2904 $\pm$ 0.1466	0.2517 $\pm$ 0.0891	-0.4891 $\pm$ 0.1528	LINER
KPG215A	Sab	-0.1434 $\pm$ 0.0328	0.0360 $\pm$ 0.1589	-0.2980 $\pm$ 0.0655	-1.4753 $\pm$ 0.3560	LINER
KPG220B	SBa	-0.1989 $\pm$ 0.0099	-0.2887 $\pm$ 0.0302	-0.3935 $\pm$ 0.0168	-1.3904 $\pm$ 0.0502	AGN
KPG222A	Sa	-0.8551 $\pm$ 0.0166	0.2688 $\pm$ 0.0138	-0.4264 $\pm$ 0.0146	-1.3003 $\pm$ 0.0321	Star-forming
KPG226A	Sa	-0.3940 $\pm$ 0.0285	-0.4566 $\pm$ 0.0566	-0.6650 $\pm$ 0.0497	-1.7715 $\pm$ 0.1479	Star-forming
KPG228A	Sa	0.6609 $\pm$ 0.0571	0.9678 $\pm$ 0.4890	0.5192 $\pm$ 0.0759	-0.5400 $\pm$ 0.1937	LINER
KPG241B	Sab	0.2447 $\pm$ 0.0812	0.2500 $\pm$ 0.1807	-0.0550 $\pm$ 0.1654	-0.9701 $\pm$ 0.4729	LINER
KPG246A	Sa	-0.2320 $\pm$ 0.0315	-0.1986 $\pm$ 0.1405	-0.3219 $\pm$ 0.0585	-1.0657 $\pm$ 0.1296	AGN
KPG252A	Sa	-0.3869 $\pm$ 0.0086	-0.3767 $\pm$ 0.0242	-0.4692 $\pm$ 0.0130	-1.4058 $\pm$ 0.0306	Star-forming
KPG255A	Sab	-0.5744 $\pm$ 0.0633	0.0659 $\pm$ 0.1759	-0.2047 $\pm$ 0.0573	-1.1323 $\pm$ 0.2016	Star-forming
KPG257B	Sab	-0.3510 $\pm$ 0.0424	-0.4617 $\pm$ 0.1430	-0.3507 $\pm$ 0.0626	-1.3867 $\pm$ 0.1455	Star-forming
KPG265B	Sa	-0.5187 $\pm$ 0.0063	-0.2686 $\pm$ 0.0157	-0.4742 $\pm$ 0.0083	-1.7040 $\pm$ 0.0328	Star-forming
KPG266A	Sab	0.2197 $\pm$ 0.0233	0.2318 $\pm$ 0.0660	0.0383 $\pm$ 0.0383	-0.6966 $\pm$ 0.0718	LINER
KPG270A	Sab	-0.3889 $\pm$ 0.0286	-0.6248 $\pm$ 0.1815	-0.5075 $\pm$ 0.0526	-1.8829 $\pm$ 0.5054	Star-forming
KPG285A	Sab	0.1228 $\pm$ 0.0315	0.3531 $\pm$ 0.1212	0.0166 $\pm$ 0.0511	-1.0220 $\pm$ 0.1804	LINER
KPG289B	Sa	-0.5191 $\pm$ 0.0108	-0.8371 $\pm$ 0.0614	-0.8041 $\pm$ 0.0242	-1.7303 $\pm$ 0.0709	Star-forming
KPG312B	S0	0.0515 $\pm$ 0.0162	-0.0333 $\pm$ 0.0438	-0.3137 $\pm$ 0.0367	-1.0605 $\pm$ 0.0770	AGN
KPG318A	Sa	-0.0607 $\pm$ 0.0213	0.1645 $\pm$ 0.0371	-0.2907 $\pm$ 0.0402	-1.3473 $\pm$ 0.1531	S-L
KPG327A	S0/a	0.1601 $\pm$ 0.0569	0.5441 $\pm$ 0.1769	0.0906 $\pm$ 0.0883	-0.8800 $\pm$ 0.2621	LINER
KPG327B	S0/a	-0.3217 $\pm$ 0.0079	-0.6363 $\pm$ 0.0345	-0.5507 $\pm$ 0.0141	-1.6678 $\pm$ 0.0495	Star-forming
KPG337A	SABa	0.0719 $\pm$ 0.0000	1.3675 $\pm$ 1.9245	-0.3788 $\pm$ 0.0559	-0.7109 $\pm$ 0.0000	Sy2
KPG342A	Sa	-0.5285 $\pm$ 0.0085	-0.3034 $\pm$ 0.0160	-0.5119 $\pm$ 0.0118	-1.8031 $\pm$ 0.0491	Star-forming
KPG348A	Sa	-0.1799 $\pm$ 0.0124	0.0827 $\pm$ 0.0168	-0.1113 $\pm$ 0.0146	-1.0213 $\pm$ 0.0319	AGN*
KPG349B	SABm	-0.2769 $\pm$ 0.0287	-0.3732 $\pm$ 0.1181	-0.2745 $\pm$ 0.0429	-1.0415 $\pm$ 0.0947	AGN
KPG355A	S0/a	-0.2799 $\pm$ 0.0102	-0.0799 $\pm$ 0.0338	-0.3937 $\pm$ 0.0173	-1.5822 $\pm$ 0.0717	AGN
KPG360A	Sab	0.1978 $\pm$ 0.0842	0.6304 $\pm$ 0.1412	0.2513 $\pm$ 0.1100	-0.4534 $\pm$ 0.1876	LINER
KPG366A	S0/a	-0.3838 $\pm$ 0.0145	-0.5970 $\pm$ 0.0743	-0.5617 $\pm$ 0.0291	-1.7457 $\pm$ 0.1496	Star-forming
KPG368A	Sa	-0.0668 $\pm$ 0.0168	0.7033 $\pm$ 0.0284	-0.2514 $\pm$ 0.0306	-0.9945 $\pm$ 0.0627	Sy2
KPG369B	Sab	-0.3745 $\pm$ 0.0043	0.0370 $\pm$ 0.0046	-0.6268 $\pm$ 0.0061	-1.5678 $\pm$ 0.0101	AGN
KPG384A	SABd	-1.2366 $\pm$ 0.0395	0.4807 $\pm$ 0.0155	-0.6179 $\pm$ 0.0234	-1.8310 $\pm$ 0.1430	Star-forming
KPG385A	Sab	-0.2753 $\pm$ 0.0144	-0.1326 $\pm$ 0.0389	-0.3423 $\pm$ 0.0224	-1.0884 $\pm$ 0.0442	AGN*
KPG395B	Sa	-0.4141 $\pm$ 0.0192	-0.5530 $\pm$ 0.1063	-0.5156 $\pm$ 0.0351	-1.7811 $\pm$ 0.2259	Star-forming
KPG400B	Sa	-0.4082 $\pm$ 0.0112	-0.7861 $\pm$ 0.0539	-0.5737 $\pm$ 0.0192	-1.8396 $\pm$ 0.1003	Star-forming
KPG413A	Sa	0.1181 $\pm$ 0.0441	0.3457 $\pm$ 0.0734	0.1669 $\pm$ 0.0605	-0.7199 $\pm$ 0.1441	LINER
KPG423A	Sab	-0.2772 $\pm$ 0.0156	-0.3584 $\pm$ 0.0750	-0.6121 $\pm$ 0.0392	-1.4676 $\pm$ 0.1124	AGN
KPG425A	SBa	-0.4318 $\pm$ 0.0080	-0.5628 $\pm$ 0.0166	-0.5251 $\pm$ 0.0114	-1.8760 $\pm$ 0.0501	Star-forming
KPG425B	S0/a	-0.0411 $\pm$ 0.0260	0.8092 $\pm$ 0.0597	-0.1732 $\pm$ 0.0475	-1.2296 $\pm$ 0.1709	Sy2
KPG437B	Sab	-0.1406 $\pm$ 0.0056	0.8404 $\pm$ 0.0079	-0.5234 $\pm$ 0.0099	-1.3326 $\pm$ 0.0184	Sy2
KPG447A	Sa	-0.3622 $\pm$ 0.0120	-0.4357 $\pm$ 0.0390	-0.4910 $\pm$ 0.0198	-1.7377 $\pm$ 0.0999	Star-forming
KPG449B	Sab	-0.1371 $\pm$ 0.0189	-0.1516 $\pm$ 0.0570	-0.2620 $\pm$ 0.0316	-1.1676 $\pm$ 0.0897	AGN
KPG455A	Sa	0.3636 $\pm$ 0.0750	0.9361 $\pm$ 59.0739	0.1912 $\pm$ 0.1196	-0.7281 $\pm$ 0.3089	LINER
KPG474B	Sa	-0.5031 $\pm$ 0.0114	-0.7489 $\pm$ 0.0666	-0.6821 $\pm$ 0.0237	-1.6340 $\pm$ 0.0783	Star-forming
KPG477B	S0	0.2623 $\pm$ 0.0419	0.4125 $\pm$ 0.1388	0.1872 $\pm$ 0.0615	-0.6152 $\pm$ 0.1262	LINER
KPG480B	S0a	0.3424 $\pm$ 0.0285	0.9104 $\pm$ 0.1547	0.0440 $\pm$ 0.0531	-0.4339 $\pm$ 0.0653	S-L
KPG495B	SBab	-0.3551 $\pm$ 0.0309	-0.9646 $\pm$ 0.5063	-0.5157 $\pm$ 0.0663	-1.3328 $\pm$ 0.1772	Star-forming
KPG496A	S0	-0.1891 $\pm$ 0.0222	0.0000 $\pm$ 0.0976	-0.4839 $\pm$ 0.0572	-1.4065 $\pm$ 0.1872	AGN
KPG150A	Sa	0.3299 $\pm$ 0.0499	0.9581 $\pm$ 0.1379	0.1766 $\pm$ 0.0791	-0.6516 $\pm$ 0.1713	LINER
KPG286B	Sa	0.6966 $\pm$ 0.2316	0.0401 $\pm$ 0.0193	-0.3559 $\pm$ 0.0159	-1.1296 $\pm$ 0.0055	AGN
KPG355B	Sa	-0.1845 $\pm$ 0.0111	-0.1347 $\pm$ 0.0255	0.0186 $\pm$ 0.0130	-0.6826 $\pm$ 0.0209	LINER
KPG368B	Sa	-0.2844 $\pm$ 0.0063	0.3010 $\pm$ 0.0084	-0.1928 $\pm$ 0.0078	-0.8456 $\pm$ 0.0102	LINER

Table A3 (cont'd)

Object	M.T. <sup>a</sup>	LOG([N II]/H $\alpha$ )	LOG([O III]/H $\beta$ )	LOG([S II]/H $\alpha$ )	LOG([O I]/H $\alpha$ )	Type
KPG378B	SABb	0.2798 $\pm$ 0.0172	0.4255 $\pm$ 0.0470	0.1171 $\pm$ 0.0268	-0.5858 $\pm$ 0.0457	LINER
KPG388B	Sab	-0.2007 $\pm$ 0.0049	0.0933 $\pm$ 0.0058	-0.3396 $\pm$ 0.0065	-0.9527 $\pm$ 0.0077	AGN
KPG398A	Sab	-0.4541 $\pm$ 0.0056	0.9582 $\pm$ 0.0055	-0.7017 $\pm$ 0.0102	-0.9831 $\pm$ 0.0096	Sy2
Sb						
KPG022B	Sbb	-0.1212 $\pm$ 0.0147	-0.1473 $\pm$ 0.0777	-0.3904 $\pm$ 0.0314	-1.4088 $\pm$ 0.1171	AGN
KPG049A	Sb	0.1339 $\pm$ 0.0282	0.4632 $\pm$ 0.0831	-0.1497 $\pm$ 0.0587	-0.8720 $\pm$ 0.1155	S-L
KPG053B	Sbb	-0.1190 $\pm$ 0.0520	0.6112 $\pm$ 0.1749	-0.2358 $\pm$ 0.1017	-1.6885 $\pm$ 0.9768	Sy2
KPG146A	Sb	-0.3627 $\pm$ 0.0189	-0.2041 $\pm$ 0.0486	-0.5772 $\pm$ 0.0351	-1.4183 $\pm$ 0.0865	AGN
KPG150B	Sb	0.2416 $\pm$ 0.0323	0.2774 $\pm$ 0.0938	0.1807 $\pm$ 0.0462	-0.6013 $\pm$ 0.0887	LINER
KPG159B	Sb	-0.3331 $\pm$ 0.0310	-0.1897 $\pm$ 0.0773	-0.3514 $\pm$ 0.0512	-1.4715 $\pm$ 0.2742	Star-forming
KPG163A	Sbc	-0.4105 $\pm$ 0.0292	-0.6588 $\pm$ 0.2047	-0.5693 $\pm$ 0.0666	-1.4852 $\pm$ 0.2231	Star-forming
KPG168B	Sc	-0.6883 $\pm$ 0.0060	-0.0187 $\pm$ 0.0075	-0.8003 $\pm$ 0.0078	-2.2243 $\pm$ 0.0307	Star-forming
KPG171A	Sbc	-0.7311 $\pm$ 0.0115	0.2867 $\pm$ 0.0141	-0.5201 $\pm$ 0.0135	-1.4738 $\pm$ 0.0332	Star-forming
KPG171B	Sb	-0.4419 $\pm$ 0.0085	-0.3946 $\pm$ 0.0230	-0.5073 $\pm$ 0.0125	-1.6458 $\pm$ 0.0451	Star-forming
KPG174A	Sbc	-0.5573 $\pm$ 0.0201	-0.3020 $\pm$ 0.0520	-0.3529 $\pm$ 0.0257	-1.3068 $\pm$ 0.0740	Star-forming
KPG178B	Sb	-0.7183 $\pm$ 0.0142	0.3040 $\pm$ 0.0150	-0.4359 $\pm$ 0.0157	-1.4182 $\pm$ 0.0422	Star-forming
KPG179B	Sb	-0.0412 $\pm$ 0.0464	0.2803 $\pm$ 0.0994	0.0372 $\pm$ 0.0623	-0.8445 $\pm$ 0.1574	S-L
KPG193B	Sb	-0.1522 $\pm$ 0.0152	0.0000 $\pm$ 0.0936	-0.3304 $\pm$ 0.0288	-1.3312 $\pm$ 0.0911	AGN
KPG200B	Sb	-0.4491 $\pm$ 0.0052	-0.1530 $\pm$ 0.0080	-0.5813 $\pm$ 0.0072	-1.8146 $\pm$ 0.0219	Star-forming
KPG205B	Sb	-0.3443 $\pm$ 0.0296	-0.4197 $\pm$ 0.1369	-0.5707 $\pm$ 0.0555	-1.5058 $\pm$ 0.0627	Star-forming
KPG206A	Sb	-0.8756 $\pm$ 0.0178	0.2553 $\pm$ 0.0124	-0.4909 $\pm$ 0.0151	-1.4872 $\pm$ 0.0417	Star-forming
KPG215B	Sb	-0.2622 $\pm$ 0.0239	0.0711 $\pm$ 0.0420	-0.5030 $\pm$ 0.0453	-1.4455 $\pm$ 0.0635	AGN
KPG216B	Sbc	-0.6998 $\pm$ 0.0110	0.1614 $\pm$ 0.0152	-0.4748 $\pm$ 0.0131	-1.5286 $\pm$ 0.0489	Star-forming
KPG219B	Sb	-0.3349 $\pm$ 0.0352	-0.6951 $\pm$ 0.1467	-0.5481 $\pm$ 0.0619	-1.6193 $\pm$ 0.0652	Star-forming
KPG225A	Sb	-0.3561 $\pm$ 0.0392	-0.4868 $\pm$ 0.0688	-0.3852 $\pm$ 0.0491	-1.2769 $\pm$ 0.0931	Star-forming
KPG225B	Sb	-0.2276 $\pm$ 0.0130	-0.3010 $\pm$ 0.0614	-0.4369 $\pm$ 0.0258	-1.2730 $\pm$ 0.0656	AGN
KPG226B	Sb	0.2264 $\pm$ 0.0506	0.0969 $\pm$ 0.0844	0.2264 $\pm$ 0.0690	-0.5540 $\pm$ 0.1575	LINER
KPG227B	Sb	-0.6104 $\pm$ 0.0110	-0.0578 $\pm$ 0.0175	-0.3952 $\pm$ 0.0128	-1.6618 $\pm$ 0.0590	Star-forming
KPG240A	Sbc	0.2991 $\pm$ 0.5267	0.9284 $\pm$ 0.1415	-0.2885 $\pm$ 0.0649	-0.5655 $\pm$ 0.1300	Sy2
KPG242A	Sb	-1.1193 $\pm$ 0.1114	0.4814 $\pm$ 0.0118	-0.6282 $\pm$ 0.0363	-1.5874 $\pm$ 0.0727	Star-forming
KPG245B	Sb	0.1627 $\pm$ 0.0400	0.3357 $\pm$ 0.1047	0.0205 $\pm$ 0.0660	-1.0810 $\pm$ 0.2713	LINER
KPG257A	Sb	-0.4876 $\pm$ 0.0266	-0.2314 $\pm$ 0.0898	-0.2550 $\pm$ 0.0296	-1.2567 $\pm$ 0.1024	Star-forming
KPG261A	Sb	-0.3536 $\pm$ 0.0225	-0.4393 $\pm$ 0.0897	-0.4580 $\pm$ 0.0416	-1.2600 $\pm$ 0.1160	Star-forming
KPG261B	Sb	-0.4749 $\pm$ 0.0354	-0.7247 $\pm$ 0.1746	-0.6270 $\pm$ 0.0707	-1.5737 $\pm$ 0.1622	Star-forming
KPG266B	Sb	-0.5208 $\pm$ 0.0195	-0.2194 $\pm$ 0.0601	-0.3808 $\pm$ 0.0269	-1.5672 $\pm$ 0.1464	Star-forming
KPG270B	Sb	0.2372 $\pm$ 0.0993	0.1943 $\pm$ 0.1247	0.2138 $\pm$ 0.1373	-0.4133 $\pm$ 0.2153	LINER
KPG283B	Sb	-1.1220 $\pm$ 0.0158	0.5031 $\pm$ 0.0121	-0.6785 $\pm$ 0.0139	-1.7420 $\pm$ 0.0507	Star-forming
KPG289A	Sb	-0.2022 $\pm$ 0.0161	-0.0746 $\pm$ 0.0431	-0.3911 $\pm$ 0.0313	-1.3118 $\pm$ 0.0922	AGN
KPG291A	Sbc	-0.2478 $\pm$ 0.0183	-0.0911 $\pm$ 0.0752	-0.3840 $\pm$ 0.0363	-1.8866 $\pm$ 0.4021	AGN
KPG293A	Sb	-0.3586 $\pm$ 0.0095	-0.3903 $\pm$ 0.0327	-0.4269 $\pm$ 0.0153	-1.5016 $\pm$ 0.0569	Star-forming
KPG294A	Sb	-0.3972 $\pm$ 0.0191	-0.2596 $\pm$ 0.0482	-0.2512 $\pm$ 0.0235	-1.4523 $\pm$ 0.1082	Star-forming
KPG296A	SBB	-0.0555 $\pm$ 0.0299	0.2300 $\pm$ 0.0682	-0.1711 $\pm$ 0.0515	-1.0046 $\pm$ 0.1286	LINER
KPG298A	Sbc	-0.1960 $\pm$ 0.0399	-0.3293 $\pm$ 0.1168	-0.4070 $\pm$ 0.0917	-1.4421 $\pm$ 0.3712	AGN
KPG298B	Sbc	0.1259 $\pm$ 0.0537	0.8943 $\pm$ 0.4159	0.0713 $\pm$ 0.0834	-0.9495 $\pm$ 0.2633	S-L
KPG299A	Sb	0.3614 $\pm$ 0.0275	0.6642 $\pm$ 0.0974	0.3055 $\pm$ 0.0377	-0.5099 $\pm$ 0.0716	LINER
KPG301A	Sb	-0.4259 $\pm$ 0.0101	-0.8002 $\pm$ 0.0459	-0.7081 $\pm$ 0.0211	-1.6543 $\pm$ 0.0636	Star-forming
KPG306B	Sb	-0.2486 $\pm$ 0.0073	-0.8852 $\pm$ 0.0379	-0.6573 $\pm$ 0.0147	-2.0341 $\pm$ 0.0968	Star-forming
KPG307A	Sb	-0.4932 $\pm$ 0.0064	-0.2756 $\pm$ 0.0094	-0.6434 $\pm$ 0.0099	-1.9298 $\pm$ 0.0341	Star-forming
KPG313A	Sbc	-0.4405 $\pm$ 0.0205	-0.5497 $\pm$ 0.0759	-0.3869 $\pm$ 0.0283	-1.5895 $\pm$ 0.1532	Star-forming
KPG313B	Sb	-0.0556 $\pm$ 0.0158	0.6717 $\pm$ 0.0276	-0.3918 $\pm$ 0.0340	-1.2583 $\pm$ 0.0855	Sy2
KPG319A	Sb	-0.9226 $\pm$ 0.0147	0.5866 $\pm$ 0.0120	-0.6614 $\pm$ 0.0167	-1.6406 $\pm$ 0.0467	Star-forming
KPG322B	Sbc	-0.2800 $\pm$ 0.0038	-0.6701 $\pm$ 0.0083	-0.6007 $\pm$ 0.0056	-1.8646 $\pm$ 0.0157	Star-forming
KPG323A	SBB	-0.5878 $\pm$ 0.0179	-0.2800 $\pm$ 0.0410	-0.3375 $\pm$ 0.0221	-1.4370 $\pm$ 0.0741	Star-forming
KPG323B	Sbc	-0.4803 $\pm$ 0.0239	-0.2004 $\pm$ 0.0598	-0.3376 $\pm$ 0.0336	-1.2207 $\pm$ 0.0834	Star-forming
KPG329B	Sb	-0.3388 $\pm$ 0.0082	-0.8493 $\pm$ 0.0334	-0.6378 $\pm$ 0.0147	-1.8235 $\pm$ 0.1893	Star-forming
KPG337B	Sb	-1.0264 $\pm$ 0.0152	0.3467 $\pm$ 0.0126	-0.6109 $\pm$ 0.0139	-1.7134 $\pm$ 0.0522	Star-forming
KPG347A	Sbc	-0.5044 $\pm$ 0.0196	-1.1862 $\pm$ 0.3571	-0.7406 $\pm$ 0.0449	-1.9546 $\pm$ 0.2896	Star-forming
KPG347B	Sbc	-0.3895 $\pm$ 0.0136	-0.4110 $\pm$ 0.0496	-0.7557 $\pm$ 0.0338	-1.9613 $\pm$ 0.1864	Star-forming

Table A3 (cont'd)

Object	M.T. <sup>a</sup>	LOG([N II]/H $\alpha$ )	LOG([O III]/H $\beta$ )	LOG([S II]/H $\alpha$ )	LOG([O I]/H $\alpha$ )	Type
KPG352A	SBb	0.0507 $\pm$ 0.0545	0.2041 $\pm$ 0.1114	-0.2545 $\pm$ 0.1282	-1.7096 $\pm$ 1.3149	S-L
KPG360B	Sb	-0.2248 $\pm$ 0.0376	-0.3919 $\pm$ 0.1875	-0.3567 $\pm$ 0.0812	-1.1835 $\pm$ 0.1990	Star-forming
KPG366B	SBb	0.3802 $\pm$ 0.0669	0.5819 $\pm$ 0.1983	0.2094 $\pm$ 0.1066	-0.4882 $\pm$ 0.1790	LINER
KPG375A	SBbc	-0.2547 $\pm$ 0.0074	-0.4952 $\pm$ 0.0257	-0.6052 $\pm$ 0.0140	-1.8573 $\pm$ 0.0695	AGN
KPG378A	Sb	0.0231 $\pm$ 0.0197	-0.0637 $\pm$ 0.0670	-0.1819 $\pm$ 0.0375	-1.2019 $\pm$ 0.1338	LINER
KPG381B	Sbc	-0.2224 $\pm$ 0.0122	0.2234 $\pm$ 0.0205	-0.3702 $\pm$ 0.0187	-1.1871 $\pm$ 0.0390	Sy1.8
KPG382A	Sbc	-0.5246 $\pm$ 0.0182	-0.6493 $\pm$ 0.0810	-0.3999 $\pm$ 0.0268	-1.3977 $\pm$ 0.0793	Star-forming
KPG395A	Sbc	-0.4479 $\pm$ 0.0164	-0.7495 $\pm$ 0.1079	-0.5490 $\pm$ 0.0293	-1.6905 $\pm$ 0.1385	Star-forming
KPG400A	Sb	-0.1371 $\pm$ 0.0348	-0.0136 $\pm$ 0.1297	-0.5150 $\pm$ 0.1049	-1.1601 $\pm$ 0.1908	AGN
KPG403B	Sb	-0.4262 $\pm$ 0.0124	-0.3931 $\pm$ 0.0558	-0.4494 $\pm$ 0.0202	-1.7366 $\pm$ 0.1136	Star-forming
KPG404B	Sb	0.2027 $\pm$ 0.0368	0.3643 $\pm$ 0.0746	0.0242 $\pm$ 0.0627	-0.7755 $\pm$ 0.1349	LINER
KPG405A	Sb	-0.5513 $\pm$ 0.0106	-0.2386 $\pm$ 0.0225	-0.4504 $\pm$ 0.0138	-1.6452 $\pm$ 0.0503	Star-forming
KPG406A	Sb	-0.5073 $\pm$ 0.0170	-0.2486 $\pm$ 0.0390	-0.3416 $\pm$ 0.0209	-1.5003 $\pm$ 0.0891	Star-forming
KPG413B	Sbc	-0.3930 $\pm$ 0.0088	-0.8571 $\pm$ 0.0582	-0.6651 $\pm$ 0.0175	-1.8924 $\pm$ 0.0907	Star-forming
KPG426B	Sb	-0.3316 $\pm$ 0.0105	-0.6744 $\pm$ 0.0464	-0.5643 $\pm$ 0.0196	-1.7752 $\pm$ 0.0979	Star-forming
KPG427B	Sb	-0.1189 $\pm$ 0.0000	-0.0786 $\pm$ 0.0981	-0.5960 $\pm$ 0.1585	-1.4024 $\pm$ 0.0000	AGN
KPG428A	SBb	-0.7162 $\pm$ 0.0286	0.0823 $\pm$ 0.0445	-0.2671 $\pm$ 0.0247	-1.3747 $\pm$ 0.0990	Star-forming
KPG430B	Sbc	-0.6538 $\pm$ 0.0130	0.1317 $\pm$ 0.0136	-0.4513 $\pm$ 0.0150	-1.4976 $\pm$ 0.0461	Star-forming
KPG433A	Sbc	-0.3162 $\pm$ 0.0105	-0.4688 $\pm$ 0.0581	-0.4791 $\pm$ 0.0196	-1.5846 $\pm$ 0.0807	Star-forming
KPG433B	Sbc	-0.4007 $\pm$ 0.0088	-0.4745 $\pm$ 0.0271	-0.6150 $\pm$ 0.0158	-1.7666 $\pm$ 0.0749	Star-forming
KPG434A	Sb	-0.1953 $\pm$ 0.0084	-0.1419 $\pm$ 0.0182	-0.4085 $\pm$ 0.0136	-1.5190 $\pm$ 0.0470	AGN
KPG440B	Sbc	-0.0786 $\pm$ 0.0000	0.5229 $\pm$ 0.1657	-0.4296 $\pm$ 0.0888	-1.3291 $\pm$ 0.0000	Sy2
KPG444A	Sbb	-0.3297 $\pm$ 0.0254	-0.3689 $\pm$ 0.1314	-0.3151 $\pm$ 0.0416	-1.2612 $\pm$ 0.1253	Star-forming
KPG453A	Sb	-0.5125 $\pm$ 0.0154	-0.9789 $\pm$ 0.1342	-0.6406 $\pm$ 0.0303	-2.6157 $\pm$ 0.9549	Star-forming
KPG455B	Sbb	0.2561 $\pm$ 0.0280	0.6353 $\pm$ 0.1704	0.0502 $\pm$ 0.0480	-0.7091 $\pm$ 0.0903	LINER
KPG458A	Sbc	-0.4771 $\pm$ 0.0172	-0.2489 $\pm$ 0.0535	-0.4462 $\pm$ 0.0266	-1.3659 $\pm$ 0.0793	Star-forming
KPG472A	Sbc	-0.9767 $\pm$ 0.0151	0.4390 $\pm$ 0.0128	-0.5645 $\pm$ 0.0143	-1.5243 $\pm$ 0.0373	Star-forming
KPG472B	Sbc	-0.4078 $\pm$ 0.0055	-0.5936 $\pm$ 0.0120	-0.6977 $\pm$ 0.0081	-2.1438 $\pm$ 0.0372	Star-forming
KPG473A	Sb	0.1025 $\pm$ 0.0128	0.6555 $\pm$ 0.0172	-0.0690 $\pm$ 0.0206	-0.7704 $\pm$ 0.0355	S-L
KPG474A	Sb	-0.5142 $\pm$ 0.0170	-0.6642 $\pm$ 0.0698	-0.7027 $\pm$ 0.0356	-1.9255 $\pm$ 0.2235	Star-forming
KPG477A	Sb	0.4227 $\pm$ 0.0844	0.1440 $\pm$ 0.1333	0.2329 $\pm$ 0.1339	-0.3647 $\pm$ 0.1966	LINER
KPG478A	Sb	-0.2775 $\pm$ 0.0192	-0.3219 $\pm$ 0.1062	-0.6253 $\pm$ 0.0499	-1.8999 $\pm$ 0.3595	AGN
KPG495A	Sb	-0.0963 $\pm$ 0.0343	-0.1120 $\pm$ 0.1161	-0.2400 $\pm$ 0.0655	-1.1265 $\pm$ 0.1882	AGN
KPG496B	Sb	-0.2829 $\pm$ 0.0181	-0.3802 $\pm$ 0.0969	-0.4329 $\pm$ 0.0346	-1.3222 $\pm$ 0.0984	AGN
KPG518A	Sb	-0.8578 $\pm$ 0.0156	0.3108 $\pm$ 0.0140	-0.4839 $\pm$ 0.0150	-1.5081 $\pm$ 0.0458	Star-forming
KPG557A	Sba	0.3193 $\pm$ 0.1119	0.1060 $\pm$ 0.1160	0.3521 $\pm$ 0.1453	-0.7773 $\pm$ 0.4971	LINER
KPG557B	Sb	-0.1795 $\pm$ 0.0276	0.1283 $\pm$ 0.0775	-0.3771 $\pm$ 0.0615	-1.7788 $\pm$ 0.5191	AGN
KPG597B	Sbc	-0.3348 $\pm$ 0.0244	-0.3667 $\pm$ 0.0791	-0.5572 $\pm$ 0.0538	-1.6819 $\pm$ 0.2660	Star-forming
Sc						
KPG021B	Sc	-0.3770 $\pm$ 0.0130	-0.3828 $\pm$ 0.0452	-0.5009 $\pm$ 0.0222	-1.6011 $\pm$ 0.0939	Star-forming
KPG052A	Sc	-0.4884 $\pm$ 0.0152	-0.8899 $\pm$ 0.1115	-0.6032 $\pm$ 0.0291	-1.6722 $\pm$ 0.1132	Star-forming
KPG156A	Sc	-0.4170 $\pm$ 0.0086	-0.9228 $\pm$ 0.0437	-0.6787 $\pm$ 0.0148	-1.9553 $\pm$ 0.0733	Star-forming
KPG156B	Sbc	-0.4136 $\pm$ 0.0665	-0.1190 $\pm$ 0.0420	-0.3272 $\pm$ 0.0417	-1.2446 $\pm$ 0.0832	Star-forming
KPG159A	Sc	-0.6847 $\pm$ 0.0131	0.1349 $\pm$ 0.0156	-0.3835 $\pm$ 0.0148	-1.3963 $\pm$ 0.0397	Star-forming
KPG168B	Sc	-0.6883 $\pm$ 0.0060	-0.0187 $\pm$ 0.0075	-0.8003 $\pm$ 0.0078	-2.2243 $\pm$ 0.0307	Star-forming
KPG178A	Sc	-0.3970 $\pm$ 0.0604	-0.6943 $\pm$ 0.2973	-0.5252 $\pm$ 0.1315	-1.8832 $\pm$ 0.5726	Star-forming
KPG220A	Sc	-0.4434 $\pm$ 0.0470	-0.3413 $\pm$ 0.0383	-0.7012 $\pm$ 0.1023	-1.8214 $\pm$ 0.1622	Star-forming
KPG230A	Sc	-0.9396 $\pm$ 0.0135	0.3703 $\pm$ 0.0124	-0.6510 $\pm$ 0.0145	-1.7235 $\pm$ 0.0484	Star-forming
KPG230B	Sc	-0.4175 $\pm$ 0.0411	-0.4150 $\pm$ 0.0402	-0.4549 $\pm$ 0.0633	-1.4852 $\pm$ 0.0857	Star-forming
KPG236A	Sc	-1.1876 $\pm$ 0.0107	0.4876 $\pm$ 0.0064	-0.8385 $\pm$ 0.0108	-2.0797 $\pm$ 0.0350	Star-forming
KPG241A	Sc	-0.4165 $\pm$ 0.0726	-1.4075 $\pm$ 2.3641	-0.4338 $\pm$ 0.1264	-1.3555 $\pm$ 0.2458	Star-forming
KPG263A	Sc	-0.1856 $\pm$ 0.0000	-0.3118 $\pm$ 0.1230	-0.4967 $\pm$ 0.0895	-1.1815 $\pm$ 0.0000	AGN
KPG272A	Sc	-0.5089 $\pm$ 0.0189	-0.2902 $\pm$ 0.0607	-0.4501 $\pm$ 0.0256	-1.6451 $\pm$ 0.1368	Star-forming
KPG272B	Sc	-0.4911 $\pm$ 0.0085	-0.6236 $\pm$ 0.0293	-0.5440 $\pm$ 0.0125	-1.7161 $\pm$ 0.0499	Star-forming
KPG280A	Sc	-0.2986 $\pm$ 0.0158	0.0736 $\pm$ 0.0430	-0.3369 $\pm$ 0.0252	-1.1528 $\pm$ 0.0542	AGN
KPG292A	Sc	-0.3666 $\pm$ 0.0051	-0.4466 $\pm$ 0.0170	-0.5041 $\pm$ 0.0076	-1.6306 $\pm$ 0.0226	Star-forming
KPG293B	Sc	-0.4792 $\pm$ 0.0082	-0.4215 $\pm$ 0.0229	-0.5214 $\pm$ 0.0126	-1.5532 $\pm$ 0.0366	Star-forming
KPG309A	Sc	-0.9356 $\pm$ 0.0372	0.4175 $\pm$ 0.0303	-0.4406 $\pm$ 0.0296	-1.3956 $\pm$ 0.0995	Star-forming

Table A3 (cont'd)

Object	M.T. <sup>a</sup>	LOG([N II]/H $\alpha$ )	LOG([O III]/H $\beta$ )	LOG([S II]/H $\alpha$ )	LOG([O I]/H $\alpha$ )	Type
KPG311B	Sc	-1.1629 $\pm$ 0.0067	0.5032 $\pm$ 0.0056	-0.9062 $\pm$ 0.0075	-2.0387 $\pm$ 0.0170	Star-forming
KPG316A	Sc	-0.4852 $\pm$ 0.0133	-0.4773 $\pm$ 0.0349	-0.4391 $\pm$ 0.0179	-1.4281 $\pm$ 0.0662	Star-forming
KPG326B	Sc	-0.8369 $\pm$ 0.0162	0.2645 $\pm$ 0.0162	-0.4116 $\pm$ 0.0164	-1.3800 $\pm$ 0.0402	Star-forming
KPG332A	Sc	-0.4636 $\pm$ 0.0049	-0.7057 $\pm$ 0.0792	-0.5754 $\pm$ 0.0290	-1.8044 $\pm$ 0.1368	Star-forming
KPG340A	Sc	-0.1040 $\pm$ 0.0138	-0.2199 $\pm$ 0.0327	-0.2439 $\pm$ 0.0229	-1.1756 $\pm$ 0.0584	AGN
KPG352B	Sc	-0.5745 $\pm$ 0.0087	-0.2580 $\pm$ 0.0165	-0.4783 $\pm$ 0.0111	-1.6564 $\pm$ 0.0344	Star-forming
KPG354B	Sc	-1.0198 $\pm$ 0.0111	0.4307 $\pm$ 0.0095	-0.6488 $\pm$ 0.0111	-1.6017 $\pm$ 0.0251	Star-forming
KPG375B	Sc	-0.4157 $\pm$ 0.0203	-0.4856 $\pm$ 0.0949	-0.6585 $\pm$ 0.0467	-1.6168 $\pm$ 0.1686	Star-forming
KPG396A	Sc	-0.6008 $\pm$ 0.0120	-0.2880 $\pm$ 0.0282	-0.4628 $\pm$ 0.0151	-1.6624 $\pm$ 0.0616	Star-forming
KPG397A	Sc	-0.8750 $\pm$ 0.0176	0.3096 $\pm$ 0.0148	-0.4922 $\pm$ 0.0159	-1.4277 $\pm$ 0.0493	Star-forming
KPG409A	Sc	-0.1843 $\pm$ 0.0350	-0.1009 $\pm$ 0.1275	-0.3476 $\pm$ 0.0711	-1.7309 $\pm$ 0.6074	AGN
KPG410A	Sc	-0.2192 $\pm$ 0.0430	-0.8206 $\pm$ 0.7114	-0.4261 $\pm$ 0.1021	-1.6475 $\pm$ 0.6513	AGN
KPG415B	Sc	-0.6773 $\pm$ 0.0144	-0.0080 $\pm$ 0.0260	-0.4111 $\pm$ 0.0166	-1.4555 $\pm$ 0.0563	Star-forming
KPG423B	Sc	-0.3710 $\pm$ 0.0097	-0.4824 $\pm$ 0.0339	-0.6073 $\pm$ 0.0173	-1.7118 $\pm$ 0.0670	Star-forming
KPG424A	Sc	-0.3510 $\pm$ 0.0058	-0.9426 $\pm$ 0.0219	-0.7013 $\pm$ 0.0094	-1.9789 $\pm$ 0.0352	Star-forming
KPG440A	Sc	-0.4141 $\pm$ 0.0307	-0.3505 $\pm$ 0.1693	-0.2034 $\pm$ 0.0349	-1.2652 $\pm$ 0.1371	Star-forming
KPG444B	Sc	-0.4339 $\pm$ 0.0117	-0.4837 $\pm$ 0.0294	-0.4150 $\pm$ 0.0167	-1.5429 $\pm$ 0.0592	Star-forming
KPG461A	Sc	-0.9182 $\pm$ 0.0144	0.4357 $\pm$ 0.0122	-0.5501 $\pm$ 0.0147	-1.5747 $\pm$ 0.0404	Star-forming
KPG511A	Sc	-0.2486 $\pm$ 0.0162	-0.5187 $\pm$ 0.1321	-0.3983 $\pm$ 0.0318	-1.8039 $\pm$ 0.2530	AGN
KPG330B	SBc	-0.8000 $\pm$ 0.1290	0.1277 $\pm$ 0.0126	1.5051 $\pm$ 0.1180	0.3939 $\pm$ 0.1383	Star-forming
Sm						
KPG212A	Sd	-1.9482 $\pm$ 0.0085	0.8194 $\pm$ 0.0041	-1.3579 $\pm$ 0.0076	-2.1572 $\pm$ 0.0113	Star-forming
KPG217A	Sd	-1.2775 $\pm$ 0.0541	0.5761 $\pm$ 0.0167	-0.7283 $\pm$ 0.0422	-1.7440 $\pm$ 0.0463	Star-forming
KPG249B	SBm	-0.5904 $\pm$ 0.0164	0.2123 $\pm$ 0.0144	-0.5536 $\pm$ 0.0210	-1.5194 $\pm$ 0.0351	Star-forming
KPG288B	SBm	-0.3851 $\pm$ 0.0048	-0.0627 $\pm$ 0.0060	-0.4600 $\pm$ 0.0064	-1.2651 $\pm$ 0.0089	AGN
KPG294B	SBm	-1.2259 $\pm$ 0.0155	0.4646 $\pm$ 0.0088	-0.6840 $\pm$ 0.0126	-1.7147 $\pm$ 0.0333	Star-forming
KPG330A	Sd	-1.0493 $\pm$ 0.0083	0.3708 $\pm$ 0.0073	-0.9699 $\pm$ 0.0106	-2.2974 $\pm$ 0.0525	Star-forming
KPG344A	Sd	-1.0957 $\pm$ 0.0093	0.2902 $\pm$ 0.0080	-0.9707 $\pm$ 0.0112	-2.4805 $\pm$ 0.0869	Star-forming
KPG349A	SBm	-0.7375 $\pm$ 0.0095	0.1800 $\pm$ 0.0082	-0.5429 $\pm$ 0.0109	-1.6739 $\pm$ 0.0325	Star-forming
KPG406B	Irr	-0.8857 $\pm$ 0.0257	0.3590 $\pm$ 0.0253	-0.4545 $\pm$ 0.0224	-1.3702 $\pm$ 0.0635	Star-forming
KPG430A	Irr	-0.4817 $\pm$ 0.0124	-0.1523 $\pm$ 0.0265	-0.4120 $\pm$ 0.0159	-1.5648 $\pm$ 0.0612	Star-forming
KPG438B	Sd	-0.9974 $\pm$ 0.0162	0.4950 $\pm$ 0.0129	-0.6597 $\pm$ 0.0161	-1.6763 $\pm$ 0.0507	Star-forming
KPG511B	Sd	-0.5686 $\pm$ 0.0141	-0.1076 $\pm$ 0.0275	-0.3915 $\pm$ 0.0182	-1.3732 $\pm$ 0.0548	Star-forming

<sup>a</sup>M.T.- Morphological Type.

\*AGN classification denotes those galaxies that are AGN according to the [N II] diagrams but not to the [S II] and/or [O I].

<sup>†</sup>L-S classification means that galaxies fall in the separation line for Seyfert and LINER according to [S II] and [O I] diagrams.

\* Type with weak broad component in permitted lines. Seyfert quantitative classification according to Winkler (1992).

